A Compressive Sensing Assisted Massive SM-VBLAST System: Error Probability and Capacity Analysis

Lixia Xiao, Pei Xiao, *Senior Member, IEEE*, Zilong Liu, Wenjuan Yu, Harald Haas, and Lajos Hanzo, *Fellow, IEEE*

***Abstract*—The concept of massive spatial modulation (SM) assisted vertical bell labs space-time (V-BLAST) (SM-VBLAST) system [1] is proposed, where SM symbols (instead of conventional constellation symbols) are mapped onto the VBLAST structure. We show that the proposed SM-VBLAST is a promising massive multiple input multiple output (MIMO) candidate owing to its high throughput and low number of radio frequency (RF) chains used at the transmitter. For the generalized massive SM-VBLAST systems, we first derive both the upper bounds of the average bit error probability (ABEP) and the lower bounds of the ergodic capacity. Then, we develop an efficient error correction mechanism (ECM) assisted compressive sensing (CS) detector whose performance tends to achieve that of the maximum likelihood (ML) detector. Our simulations indicate that the proposed ECM-CS detector is suitable both for massive SM-MIMO based point-to-point and for uplink communications at the cost of a slightly higher complexity than that of the compressive sampling matching pursuit (CoSaMP) based detector in the high SNR region.**

***Index Terms*—Spatial modulation (SM), Multiple-Input Multiple-Output (MIMO), Vertical Bell Labs Space-Time (VBLAST), Compressive Sensing (CS), Average Bit Error Probability (ABEP), Capacity analysis.**

I. Introduction

A. Background

L. Xiao, P. Xiao, W. Yu, are with University of Surrey 5GIC.

Z. Liu is with the School of Computer Science and Electronic Engineering, University of Essex, UK, CO4 3SQ

L. Hanzo are with the school of Electronics and Computer Science, University of Southampton, Southampton SO17 1BJ, U.K. (email: lh@ecs.soton.ac.uk).

H. Hass is with Electronics and Electrical Engineering, University of Edinburgh.

This work was supported by the U.K. Engineering and Physical Sciences Research Council under Grant EP/N020391/1. The authors also would like to acknowledge the support of the University of Surrey 5GIC (http://www.surrey.ac.uk/5gic) members for this work.

The work of Z. Liu was supported in part by the EPSRC Project: New Air Interface Techniques for Future Massive Machine Communications under Grant EP/P03456X/1, in part by the H2020 EU-Taiwan Project: Converged Wireless Access for Reliable 5G MTC for Factories of Future -Clear5G (61745), and in part by the National Natural Science Foundation of China through the Research Fund for International Young Scientists under Grant 61750110527.

L. Hanzo would like to acknowledge the financial support of the ERC Advanced Fellow Grant Quantcom.

THE massive multiple-input multiple-output (MIMO) transmission technique [2]-[3], which employs a multiplicity transmit/receive antennas has been considered to be one of the key techniques for future wireless communications. Three popular classes of massive MIMO communication scenarios have attracted attention [2]: point-to-point (P2P) communication, where both the transmitter and receiver employ numerous antennas, as well as uplink (UL) and downlink (DL) communications, where many more antennas are employed by the base station (BS) than by the individual users. Conventional MIMO solutions, e.g., VBLAST and space-time block codes (STBC) [4] [6], tend to require a large number of radio frequency (RF) chains, hence imposing a substantial implementation cost and signal processing complexity in massive MIMO channels. In contrast, spatial modulation (SM) based MIMO systems [6]-[9], which employs the indices of the activated antennas as an additional means of implicitly conveying information, is a promising low-cost massive MIMO candidate for next generation wireless communications [10]-[35].

The existing state-of-the-art of massive SM-MIMO systems is mainly focused on UL communications [11]-[25], where each user invokes SM to convey information and the BS employs multi-user detection to recover the transmit messages. Specifically, in [11]-[16], the advantages of massive SM-MIMO systems have been demonstrated in terms of their spectral-, energy- and cost-efficiencies. Message passing (MP) algorithms based multiuser detectors have been conceived [17]-[20] for massive SM-MIMO systems communicating both over narrowband and broadband channels. Furthermore, low-complexity compressive sensing (CS) detectors have been developed in [21]-[22], which exhibited a modest performance erosion. Recently, the performance of massive SM-MIMO systems have also been studied in the context of visible light [23], non-orthogonal multiple access (NOMA) [24] and physical layer encryption communication scenarios [25].

Massive SM-MIMO systems designed both for DL and P2P communication scenarios have been studied in [26]-[35]. However, these systems are mainly designed for activating only a few antennas. Naturally, the number of transmit antenna combinations (TACs) is determined by the number of antennas N_u activated during each symbol slot. When both N_u and the number of transmit antennas

(TA) N_t increases, finding an efficient bit-to-symbol mapping and demapping may not be easy for a high number of TACs [36]. To circumvent this issue, antenna group based massive SM-MIMO schemes have been developed independently in [1] and [35], where the TAs are divided into multiple small groups and SM is employed in each group. In this treatise we refer to the scheme of [1] as SM-VBLAST. In an SM-VBLAST system, the information bits are conveyed by N_u sub-indices (instead of a single activated index), hence the complexity of mapping and demapping is comparable to that of the conventional SM scheme. It has been shown in [1] that SM-VBLAST is capable of providing substantial performance gains over both the conventional generalized SM (GSM) [8] and the VBLAST systems at an identical number of RF chains. This compelling benefit equips the SM-VBLAST system with the unique ability to support massive MIMO based P2P, UL and DL communications.

B. Motivations and Contributions of This Work

Theoretical analysis of Average Bit Error Probability (ABEP) for massive SM-VBLAST is more complex than that for its small-scale counterpart. The ABEP upper bound of massive SM-VBLAST for $M = 1$, where $\log_2(M)$ refers to the number of information bits sent by each SM symbol (in addition to that conveyed by the indices of the activated TAs), has been derived in [1]. In this case, each SM-VBLAST symbol is consisted of N_u Space Shift Keying (SSK) symbols. When $M > 1$, however, the derivation approach in [1] for the ABEP upper bound may not be applicable. The upper bound of the ABEP for small-scale GSM associated with $M > 1$ has been derived in [7], but the complexity of the ABEP calculation is in the order of 2^B, where B denotes the transmit rate of the GSM system. For massive SM-VBLAST, for example, the value of B may be as high as 320 bits per channel use (bpcu) for the settings of $N_t = 320$, $N_u = 80$ and $M = 4$, which makes the ABEP calculation prohibitively challenging.

To the best of our knowledge, the closed-forms of the Average Bit Error Probability (ABEP) expressions and the capacity of UL massive MIMOs relying on a large number of users have not been investigated. Although the ABEP of massive SM-MIMO supporting a low number of users has been studied in [17], it may not be straightforward to extend it to a large number of users and/or receiver antennas (RAs). In conventional GSM systems, the ergodic capacity performances have been studied in [37]-[38] for small-scale SM-MIMO only, but these approaches may not be suitable for the capacity analysis of massive SM-VBLAST.

Additionally, designing low-complexity CS capable of approaching the optimal performance at an acceptable complexity is still a challenging open issue [39]. It is worth pointing out that massive SM-VBLAST transmit signals exhibit inherent sparsity, which can be efficiently exploited by CS algorithms. The existing CS algorithms designed for massive SM-MIMO, such as Orthogonal Matching Pursuit (OMP) [40], Compressive Sampling Matching Pursuit (CoSaMP) [21] and MP [17]-[20] fail to strike an attractive performance vs. complexity trade-off. This motivates us to design an enhanced CS algorithm for massive SM-VBLAST systems.

Against the above background, the contributions of this paper are summarized as follows:

1) We analyze the ABEP of a massive SM-VBLAST system for generalized amplitude phase modulation (APM) schemes and derive a closed form ABEP upper bound for SM-VBLAST using low-order APM schemes, such as BPSK and QPSK.
2) We derive a lower bound of the ergodic capacity of massive SM-VBLAST systems and validate it through Monte Carlo simulations. Both our theoretical and simulation results indicate that the capacity of the massive SM-VBLAST system is significantly higher than that of the conventional VBLAST systems with an identical number of RF chains.
3) We develop an efficient Error Correction Mechanism (ECM) assisted CS detector for massive SM-VBLAST systems having large N_t and N_u. Our proposed ECM assisted CS detectors are capable of approaching the error rate performance of the maximum likelihood (ML) detector by efficiently identifying and correcting the errors of the transmit indices encountered in the conventional CS detector at a low complexity.
4) We show that the closed-form ABEP expression derived and the ergodic capacity, as well as the ECM-CS detector are also applicable for UL massive SM-MIMO systems. We present the ABEPs of massive UL SM-MIMO systems having $N_u = 40, N_r = 128$ and $N_u = 80, N_r = 256$, where N_u and N_r are the number of users and the number of antennas in the BS, respectively. It is shown that the performance of our proposed ECM assisted CS detector approach that of the ML detector in these UL setups, despite only imposing a slightly higher complexity than that of the CoSaMP based detector.
5) We reveal that for a P2P communication system, the throughput of ECM-assisted massive SM-VBLAST can be hundreds or thousands bpcu but at a reduced number RF chains and a reduced complexity.

Notations: $\|\cdot\|^2$ denotes the Frobenious norms of a matrix, while $|\cdot|$ represents the magnitude of a complex quantity; $(\cdot)^T$ and $(\cdot)^H$ stand for the transpose and the Hermitian transpose of a vector/matrix, respectively. $A \backslash B$ denotes removing the set B from the set A and $A \cup B$ denotes adding the set B into the set A.

II. Massive SM-VBLAST System

A. System model of P2P communication

The system model of the P2P SM-VBLAST system is shown in Fig. 1 (a). According to [1], the information bits of $B = \sum_{l=1}^{N_u} B_l$ are partitioned into N_u ($1 \leq N_u \leq N_t/2$) groups. The l-th block of information bits $B_l =$

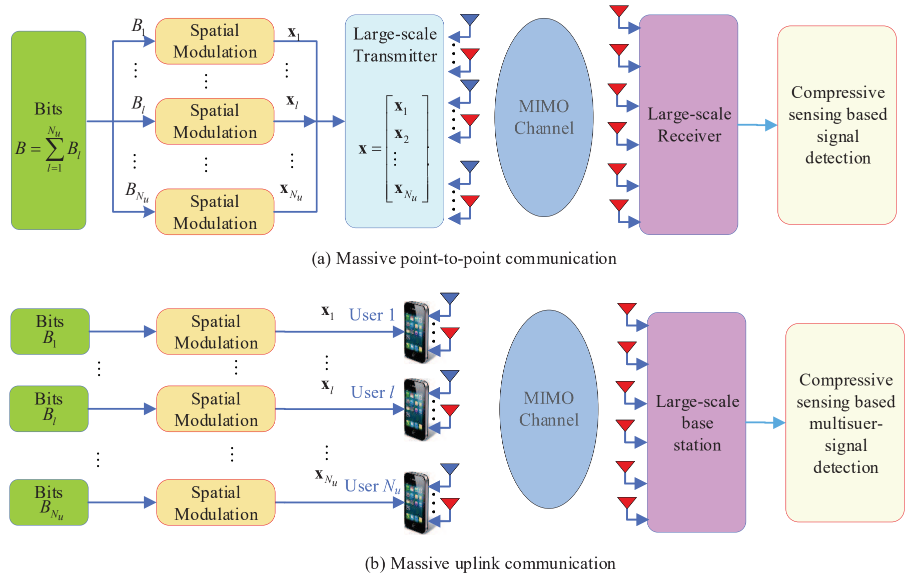

Fig. 1. Proposed compressive sensing based massive SM-VBLAST systems: a) Massive P2P communication; b) Massive UL communication.

$\log_2(N_{sm}^l)+\log_2(M_l)$ can be mapped into a SM symbol having M_l-PSK symbols and N_{sm}^l TAs as

$$\mathbf{x}_l = [\underbrace{0,...,0}_{q_l-1}, s_l, \underbrace{0,...,0}_{N_{sm}^l-q_l}]^T, \tag{1}$$

where q_l is the antenna index of the l-th SM symbol. Then, the transmitted signal can be expressed as

$$\begin{aligned}\mathbf{x} &= [\mathbf{x}_1^T, \mathbf{x}_2^T, ..., \mathbf{x}_{N_u}^T]^T \\ &= [\underbrace{0,...,0}_{q_1-1}, s_1, \underbrace{0,...,0}_{N_{sm}^1-q_1}, ..., \underbrace{0,...,0}_{q_{N_u}-1}, s_{N_u}, \underbrace{0,...,0}_{N_{sm}^{N_u}-q_{N_u}}]^T .\end{aligned} \tag{2}$$

The relationship between the l-th activated index k_l in $\mathbf{x}$ and q_l is expressed as

$$k_l = \sum_{j=1}^{l-1} N_{sm}^j + q_l. \tag{3}$$

Let $\mathbf{H}\in\mathbb{C}^{N_r\times N_t}$ and $\mathbf{n}\in\mathbb{C}^{N_r\times 1}$ be the MIMO channel matrix and noise matrix, whose entries have complex-valued Gaussian distributions of $\mathcal{CN}(0,1)$ and $\mathcal{CN}(0,\sigma^2)$, respectively. The received signal $\mathbf{y}\in\mathbb{C}^{N_r\times 1}$ is written as

$$\mathbf{y} = \mathbf{H}\mathbf{x} + \mathbf{n} = \mathbf{H}_A\mathbf{s} + \mathbf{n}, \tag{4}$$

where $\mathbf{H}_A = (\mathbf{h}_{k_1}, \mathbf{h}_{k_2}, ..., \mathbf{h}_{k_{N_u}})$ is the sub-matrix of $\mathbf{H}$ with N_u columns, and $\mathbf{s}=(s_1,...,s_{N_u})^T$ is the transmit symbol vector corresponding to the TAC $A=(k_1,...,k_{N_u})$.

According to [1], the optimal ML detector is formulated as

$$(\hat{I}, \hat{\mathbf{s}})_{\mathrm{ML}} = \arg\min_{A\in\mathbb{A}, \mathbf{s}\in\mathbb{S}} \|\mathbf{y}-\mathbf{H}_A\mathbf{s}\|^2, \tag{5}$$

where $\mathbb{A}$ is a TAC set having a size of $N=\prod_{l=1}^{N_u} N_{sm}^l$, and $\mathbb{S}$ is the set of N_u-element symbol vectors.

B. System model of UL communication

The system model of the UL SM-VBLAST system is shown in Fig. 1 (b). In UL communication, N_u denotes the number of users and N_{sm}^l represents the number of TAs of the l-th user. Each user employs SM transmission using N_{sm}^l TAs and M_l-PSK modulation. At the base station, the signal received by r-th ($r=1,...,N_r$) RA is expressed as

$$y_r = \sum_{l=1}^{N_u} \mathbf{h}_{r,l}\mathbf{x}_l + n_r, \tag{6}$$

where $\mathbf{h}_{r,l}\in\mathbb{C}^{1\times N_{sm}^l}$ can be considered as a subset of $\mathbf{H}$ of (4). The received signal of the base station in UL communication is $\mathbf{Y}=[y_1,...,y_{N_r}]$, which is the same as (4). Therefore, the ABEP analysis and signal detection in this paper are suitable for both P2P and UL communication. In order to make the system models more explicit, the notations of P2P and UL communication are concluded in Table I.

III. Generalized ABEP Analysis of Massive SM-VBLAST Systems

In this section, the ABEP of massive SM-VBLAST associated with $M_l>1$ [1] is formulated as

$$\begin{aligned}P_b &= \frac{1}{B2^B}\sum_{i=1}^{2^B}\sum_{j\neq i}^{2^B} d(\mathbf{x}^i,\mathbf{x}^j)P(\mathbf{x}^i\to\mathbf{x}^j) \\ &\approx \frac{1}{B}\sum_{j=2}^{2^B} d(\mathbf{x}^1,\mathbf{x}^j)P(\mathbf{x}^1\to\mathbf{x}^j),\end{aligned} \tag{7}$$

where $P(\mathbf{x}^1\to\mathbf{x}^j)$ denotes the Pairwise Error Probability (PEP), $d(\mathbf{x}^1,\mathbf{x}^j)$ is the Hamming Distance (HD) associated with the corresponding PEP event. Specifically, we have $\mathbf{x}^1=[(\mathbf{x}_1^1)^T,...,(\mathbf{x}_{N_u}^1)^T]^T$ and $\mathbf{x}^j=[(\mathbf{x}_1^j)^T,...,(\mathbf{x}_{N_u}^j)^T]^T$, $j=(1,...,2^B)$, which are associated with information bits

[1]Eq. (7) holds for BPSK, QPSK, as well as for gray coding aided M_l-PSK modulation. Hence, the ABEP analysis of this paper mainly aims for characterizing M_l-APM satisfying Eq. (7).

TABLE I
NOTATIONS FOR P2P AND UL COMMUNICATION.

Parameter	P2P communication	UL communication
N_t	The number of TAs	The number of TAs of all the users
N_u	The number of RF chains	The number of users
N_{sm}^l	The number of TAs of l-th level	The number of TAs of the l-th user
k_l	The index of the l-th activated TA	The activated TA index of the l-th user
$\mathbf{x}_l$	The SM symbol of the l-th level	The transmit SM symbol of the l-th user
N_r	The number of RAs	

as

$$\begin{aligned}&\mathbf{b}^1 = [\underbrace{0,...,0}_{\mathbf{b}_1^1},\cdots,\underbrace{0,...,0}_{\mathbf{b}_{N_u}^1}] \to \mathbf{x}^1,\\ &\mathbf{b}^j = [\underbrace{c_1^1,...,c_1^{B_1}}_{\mathbf{b}_1^j},\cdots,\underbrace{c_{N_u}^1,...,c_{N_u}^{B_{N_u}}}_{\mathbf{b}_{N_u}^j}] \to \mathbf{x}^j \ .\end{aligned} \tag{8}$$

According to [1], the PEP event can be defined as

$$P(\mathbf{x}^1 \to \mathbf{x}^j) = F(\bar{\zeta}) = \gamma(\bar{\zeta})^{N_r} \sum_{k=0}^{N_r-1} \left(\begin{array}{c} N_r-1+k \\ k \end{array} \right) \left[1-\gamma\left(\bar{\zeta}\right)\right]^k \tag{9}$$

where $\gamma\left(\bar{\zeta}\right) = \frac{1}{2}\left(1-\sqrt{\frac{\bar{\zeta}/2}{1+\bar{\zeta}/2}}\right)$, and $\bar{\zeta}$ is the mean value of $\zeta = \|\mathbf{H}(\mathbf{x}^1-\mathbf{x}^j)\|^2/2\sigma^2$ associated with $N_r = 1$ as

$$\bar{\zeta} = \mathbb{E}\{\mathbf{H}(\mathbf{x}^1-\mathbf{x}^j)^2/2\sigma^2|N_r=1\} \quad = \|\mathbf{x}^1-\mathbf{x}^j\|^2/2\sigma^2. \tag{10}$$

According to (8), there are only T different values of $\bar{\zeta}$ in (10) which are named as $\bar{\zeta}_1$,...,$\bar{\zeta}_T$. Hence, Eq. (7) can be simplified to

$$P_b = D(\bar{\varsigma}_1)F(\bar{\varsigma}_1) + D(\bar{\varsigma}_2)F(\bar{\varsigma}_2) + \cdots + D(\bar{\varsigma}_T)F(\bar{\varsigma}_T), \tag{11}$$

where $D(\bar{\varsigma}_t)$ denotes the Average HD (AHD) associated with $\bar{\varsigma}_t$. Since the values of $F(\bar{\zeta}_1)$,...,$F(\bar{\zeta}_T)$ are easy to calculate from (9), the calculation of $D(\bar{\varsigma}_1),...,D(\bar{\varsigma}_T)$ is the key issue in the ABEP evaluation.

A. Generalized ABEP Analysis

According to (8), The HD between $\mathbf{x}_l^j$ and $\mathbf{x}_l^1$ $l = (1,...,N_u)$ can be expressed as

$$d_l^{p_l} = \mathrm{setdiff}(\mathbf{b}_l^j, \mathbf{b}_l^1) \in [0,1,...,B_l] \ , \tag{12}$$

where setdiff$(\mathbf{x},\mathbf{y})$ is a function returning the difference between $\mathbf{x}$ and $\mathbf{y}$, while $p_l = \|\mathbf{x}_l^1 - \mathbf{x}_l^j\|^2$ is expressed as

$$p_l = \begin{cases} \phi_{M_l}, \text{ if } q_l^1 = q_l^j \\ 2, \text{ else} \end{cases}, l = 1, \cdots N_u, \tag{13}$$

where ϕ_{M_l} denotes the Euclidean Distance (ED) between any two M_l-APM symbols. Upon considering BPSK and QPSK for example, ϕ_{M_l} is expressed as

$$\phi_{M_l} = \begin{cases} (0,4), \text{ BPSK}, \\ (0,2,4), \text{ QPSK}, \end{cases} \tag{14}$$

Then the mean value of ζ and AHD are formulated as

$$\begin{aligned}&\bar{\varsigma}_t = \|\mathbf{x}^1-\mathbf{x}^j\|^2/(2\sigma^2) = \sum_{l=1}^{N_u} p_l/(2\sigma^2) = t/\sigma^2,\\ &D(\bar{\varsigma}_t) = \frac{1}{B}\left[\sum_{\forall(p_1+\cdots+p_{N_u}=2t)} (d_1^{p_1}+d_2^{p_2}+\cdots d_{N_u}^{p_{N_u}})\right].\end{aligned} \tag{15}$$

Hence, how to find the common values of $\bar{\varsigma}_t$ and their corresponding HDs become the key issue in the calculation of $D(\bar{\varsigma}_t)$. According to (14) and (15), there are some common values of p_l in each level. Assuming that $N_l^{p_l}$ is the number of common values p_l, $(l = 1,2...,N_u)$, (15) can be represented as

$$D(\bar{\varsigma}_t) = \frac{\sum\limits_{\forall(p_1+\cdots+p_{N_u}=2t)} \sum\limits_{i_1=1}^{N_1^{p_1}} \cdots \sum\limits_{i_{N_u}=1}^{N_{N_u}^{p_{N_u}}} \left(d_1^{p_1,i_1}+\cdots+d_{N_u}^{p_{N_u},i_{N_u}}\right)}{B}, \tag{16}$$

with

$$\begin{aligned}&\sum_{i_1=1}^{N_1^{p_1}} \cdots \sum_{i_{N_u}=1}^{N_{N_u}^{p_{N_u}}} \left(d_1^{p_1,i_1}+\cdots+d_{N_u}^{p_{N_u},i_{N_u}}\right)\\ &= \prod_{l=2}^{N_u} N_l^{p_l} \sum_{i_1=1}^{N_1^{p_1}} d_1^{p_1,i_1} + \prod_{l=1,l\neq 2}^{N_u} N_l^{p_l} \sum_{i_2=1}^{N_2^{p_2}} d_2^{p_2,i_2} +\\ &\prod_{l=1,l\neq 3}^{N_u} N_l^{p_l} \sum_{i_3=1}^{N_3^{p_3}} d_3^{p_3,i_3} + \cdots + \prod_{l=1}^{N_u-1} N_l^{p_l} \sum_{i_{N_u}=1}^{N_{N_u}^{p_{N_u}}} d_{N_u}^{p_{N_u},i_{N_u}}\\ &= \prod_{l=2}^{N_u} N_l^{p_l} D_1^{p_1} + \prod_{l=1,l\neq 2}^{N_u} N_l^{p_l} D_2^{p_2} + \cdots + \prod_{l=1}^{N_u-1} N_l^{p_l} D_{N_u}^{p_{N_u}},\end{aligned} \tag{17}$$

where $D_l^{p_l}$ denotes the total HDs associated with p_l as $D_l^{p_l} = \sum\limits_{i_l=1}^{N_l^{p_l}} d_l^{p_l,i_l}$. As a result, the values of $N_l^{p_l}$ and $D_l^{p_l}$ become important for calculating (16), which are associated with specific antenna configurations. Considering BPSK and QPSK for example, we have $p_l = [0,2,4]$. The values of $N_l^{p_l}$ and $D_l^{p_l}$ can be obtained by

$$\begin{aligned}&\text{BPSK} \to \begin{cases} N_l^0 = 1, D_l^0 = 0, \\ N_l^2 = 2(N_{sm}^l - 1), D_l^2 = \sum\limits_{b=1}^{B_l} bC_{B_l}^b - 1, \\ N_l^4 = 1, D_l^4 = 1, \end{cases}\\ &\text{QPSK} \to \begin{cases} N_l^0 = 1, D_l^0 = 0, \\ N_l^2 = 4(N_{sm}^l - 1)+2, D_l^2 = \sum\limits_{b=1}^{B_l} bC_{B_l}^b - 2 \\ N_l^4 = 1, D_l^4 = 2. \end{cases}\end{aligned} \tag{18}$$

Based on the values of $N_l^{p_l}$ and $D_l^{p_l}$, the ABEP of the massive SM-VBLAST system using $M_l > 1$ is presented in **Algorithm 1**, where unique$(\cdot)$, find$(\cdot)$ and length$(\cdot)$ are the standard MATLAB functions.

In summary, for any M_l-APM symbol based massive SM-VBLAST system, the value of $N_l^{p_l}$ and $D_l^{p_l}$ can be obtained by (18). According to (9), (11), (16) and (17),

Algorithm 1 ABEP of the large-scale SM-VBLAST system with $M > 1$

Input: $B = \sum_{l=1}^{N_u} B_l$, $P_b = 0$ $\bar{\varsigma} = \phi$, $D_{\bar{\varsigma}} = \phi$;
Output: P_b;
for $p_1 \in \phi_{M_1} \cup \{2\}$ **do**
  Obtain $N_1^{p_l}$ and $D_1^{p_l}$ according to (18);
  for $p_2 \in \phi_{M_2} \cup \{2\}$ **do**
    Obtain $N_2^{p_2}$ and $D_2^{p_2}$ according to (18);
    ...
    for $p_{N_u} \in \phi_{M_{N_u}} \cup \{2\}$ **do**
      Obtain $N_{N_u}^{p_{N_u}}$ and $D_{N_u}^{p_{N_u}}$ according to (18);
      $E = (p_1 + p_2 + p_3 + \cdots + p_{N_u})/2\sigma^2$;
      Calculate the AHD value D by (16) and (17).
      $\bar{\varsigma} = \{\bar{\varsigma}\} \cup \{E\}$;
      $D_{\varsigma} = \{D_{\varsigma}\} \cup \{D\}$;
    end for
    ...
  end for
end for
$C = \text{unique}(\bar{\varsigma})$;
$T = \text{length(C)}$;
for $t \in (1, T)$ **do**
  $\bar{\varsigma}_t = C(t)$
  $t_{\text{index}} = \text{find}(\bar{\varsigma} = C(t))$;
  $D(\bar{\varsigma}_t) = \sum_{i \in t_{\text{index}}} D_{\varsigma}(i)$;
  Obtain $F(\bar{\varsigma}_t)$ by (9).
  $P_b = P_b + F(\bar{\varsigma}_t) * D(\bar{\varsigma}_t)$.
end for

the generalized ABEP of any M_l-APM symbols can be calculated by **Algorithm 1**. Based on **Algorithm 1**, assuming that $N_{\phi_{M_l}}$ is the size of ϕ_{M_l}, the complexity order of the ABEP calculation is $O(N_{\phi_{M_l}}^{N_u})$, which is independent of N_t. As $N_{\phi_{M_l}}$ and N_u increase, the complexity of ABEP calculation still becomes excessive. Next, a closed form of the ABEP of massive SM-VBLAST associated with low-order APM symbols is derived.

B. Low-Complexity ABEP Analysis

In this section, the closed form of the ABEP upper bound is derived for massive SM-VBLAST using $M_l = 2$ and $M_l = 4$. For the cases of $M_l > 4$, the closed form of the upper bound becomes more complex and will be considered as our future work. Since $\phi_{M_l} = [0, 2, 4]$ holds true for $M_l = 2$ and $M_l = 4$, the value of $t \in [1, ..., 2N_u]$ in (15) is dominated by the number of $0, 2, 4$ in $(p_1, p_2, ..., p_{N_u})$. Assuming that κ_0, κ_2 and κ_4 are the total number of $0, 2, 4$ in $(p_1, p_2, ..., p_{N_u})$, the relationship among them can be presented by

$$2t = \sum_{l=1}^{N_u} p_l = 0 \times \kappa_0 + 2 \times \kappa_2 + 4 \times \kappa_4, \kappa_0 + \kappa_2 + \kappa_4 = N_u, \tag{19}$$

hence we have $\kappa_2 = t - 2\kappa_4$, $\kappa_0 = N_u - t + \kappa_4$. For a certain combination of κ_2 and κ_4, there is a total of $C_{N_u}^{\kappa_2} C_{N_u-\kappa_2}^{\kappa_4} C_{\kappa_0}^{\kappa_0}$ scenarios that satisfy (19). Considering $N_u = 4$, $\kappa_2 = 2$ and $\kappa_4 = 1$ for example, there are 12 scenarios having $p_1 + p_2 + p_3 + p_4 = 8$, which are

$$\begin{aligned} &p_1{=}p_2{=}2, p_3{=}4, p_4{=}0; p_1{=}p_2{=}2, p_3{=}0, p_4{=}2; \\ &p_1{=}p_3{=}2, p_2{=}4, p_4{=}0; p_1{=}p_3{=}2, p_2{=}0, p_4{=}4; \\ &p_1{=}p_4{=}2, p_2{=}4, p_3{=}0; p_1{=}p_4{=}2, p_2{=}0, p_3{=}4; \\ &p_2{=}p_3{=}2, p_1{=}4, p_4{=}0; p_2{=}p_3{=}2, p_1{=}0, p_4{=}4; \\ &p_2{=}p_4{=}2, p_1{=}4, p_3{=}0; p_2{=}p_4{=}2, p_1{=}0, p_3{=}4; \\ &p_3{=}p_4{=}2, p_1{=}4, p_2{=}0; p_3{=}p_4{=}2, p_1{=}0, p_2{=}4. \end{aligned} \tag{20}$$

Assuming that $p_{l_1} = \cdots = p_{l_{\kappa_2}} = 2, p_{l_{\kappa_2+1}} = \cdots = p_{l_{\kappa_2+\kappa_4}} = 4$, according to (16)-(17), the HDs of one of the cases are expressed as

$$\begin{aligned} H_{(\kappa_2,\kappa_4)} &= \sum_{i_1=1}^{N_{l_1}^2} \cdots \sum_{i_{\kappa_2}=1}^{N_{l_{\kappa_2}}^2} \sum_{i_{\kappa_2+1}=1}^{N_{l_{\kappa_2+1}}^4} \cdots \sum_{i_{\kappa_2+\kappa_4}=1}^{N_{l_{\kappa_2+\kappa_4}}^4} \Big(d_{l_1}^{2,i_1} + \cdots + \\ & d_{l_{\kappa_2}}^{2,i_{\kappa_2}} + d_{l_{\kappa_2+1}}^{4,i_{\kappa_2+1}} + \cdots + d_{l_{\kappa_2+\kappa_4}}^{4,i_{\kappa_2+\kappa_4}} \Big) \\ &= \prod_{u=2}^{\kappa_2} N_{l_u}^2 \prod_{v=\kappa_2+1}^{\kappa_2+\kappa_4} N_{l_v}^4 D_{l_1}^2 + \cdots \prod_{u=1}^{\kappa_2-1} N_{l_u}^2 \prod_{v=\kappa_2+1}^{\kappa_2+\kappa_4} N_{l_v}^4 D_{l_{\kappa_2}}^2 \\ &+ \cdots + \prod_{u=1}^{\kappa_2} N_{l_u}^2 \prod_{v=\kappa_2+1}^{\kappa_2+\kappa_4-1} N_{l_v}^4 D_{l_{\kappa_2+\kappa_4}}^4. \end{aligned} \tag{21}$$

Since there are $C_{N_u}^{\kappa_2} C_{N_u-\kappa_2}^{\kappa_4}$ scenarios for this case, the total HDs associated with $\sum_{l=1}^{N_u} p_l = 2\kappa_2 + 4\kappa_4$ can be expressed as

$$H_{(\kappa_2,\kappa_4)}^{all} = \sum_{(l_1 \cdots l_{\kappa_2}) \in I_{N_u}^{\kappa_2}} \; \sum_{(l_{\kappa_2+1} \cdots l_{\kappa_2+\kappa_4}) \in \tilde{I}_{N_u-\kappa_2}^{\kappa_4}} H_{(\kappa_2,\kappa_4)}, \tag{22}$$

where $I_{N_u}^{\kappa_2}$ denotes the Index Combination Set (ICS) that consists of choosing κ_2 indices from $(1, 2, ..., N_u)$, while $\tilde{I}_{N_u-\kappa_2}^{\kappa_4}$ represents the ICS consisting of choosing κ_4 indices from $\{(1, 2, ..., N_u)\backslash I_{N_u}^{\kappa_2}\}$. Taking $N_u = 4$, $\kappa_2 = 2$ and $\kappa_4 = 1$ for example, the sets $I_{N_u}^{\kappa_2}$ and $\tilde{I}_{N_u-\kappa_2}^{\kappa_4}$ are expressed as

$$I_4^{\kappa_2} = \{ \underbrace{(1,2)}_{\tilde{I}_2^{\kappa_4}=\{3,4\}}, \underbrace{(1,3)}_{\tilde{I}_2^{\kappa_4}=\{2,4\}}, \underbrace{(1,4)}_{\tilde{I}_2^{\kappa_4}=\{2,3\}}, \underbrace{(2,3)}_{\tilde{I}_2^{\kappa_4}=\{1,4\}}, \underbrace{(2,4)}_{\tilde{I}_2^{\kappa_4}=\{1,3\}}, \underbrace{(3,4)}_{\tilde{I}_2^{\kappa_4}=\{1,2\}} \}. \tag{23}$$

The above HD analysis is based on a certain combination of κ_2 and κ_4. However, according to (19), different values of κ_2 and κ_4 can result in a common value of t. Hence, the calculation of AHD $D(\bar{\varsigma}_t)$ associated with the event $\sum_{l=1}^{N_u} p_l = 2t$ will be determined by all the different combinations of κ_2 and κ_4. Next, how to obtain the combinations of κ_2 and κ_4 for different values of t will be discussed in four cases: 1) t is even with $t \leq N_u$; 2) t is odd with $t \leq N_u$; 3) t is even with $t > N_u$ and 4) t is odd with $t > N_u$.

Case 1 - t is even with $t \leq N_u$: For this case, the values of $(p_{l_1}, ..., p_{l_{N_u}})$ satisfying $\sum_{l=1}^{N_u} p_l = 2t$ are given by

$$\begin{cases} \{\underbrace{p_{l_1}, \cdots, p_{l_t}}_{2 \to \kappa_2 = t}, \underbrace{p_{l_{t+1}}, \cdots, p_{l_{N_u}}}_{0 \to \kappa_0 = N_u - t}\}, \\ \vdots \\ \{\underbrace{p_{l_1}, \cdots, p_{l_{t/2}}}_{4 \to \kappa_4 = t/2}, \underbrace{p_{l_{t/2+1}}, \cdots, p_{l_{N_u}}}_{0 \to \kappa_0 = N_u - t/2}\}, \end{cases} \tag{24}$$

where $l_1, ..., l_{N_u} \in (1, N_u)$. Observe from (24) that the

$$
\begin{aligned}
BD(\varsigma^{even}_{t\le N_u}) &= \sum_{\kappa_4=0}^{t/2} C_{N_u}^{t-2\kappa_4} C_{N_u-(t-2\kappa_4)}^{\kappa_4}[(t-2\kappa_4)(N_l^2)^{t-2\kappa_4-1}(N_l^4)^{\kappa_4}D_l^2+\kappa_4(N_l^2)^{t-2\kappa_4}(N_l^4)^{\kappa_4-1}D_l^4],\\
BD(\varsigma^{odd}_{t\le N_u}) &= \sum_{\kappa_4=0}^{(t-1)/2} C_{N_u}^{t-2\kappa_4} C_{N_u-(t-2\kappa_4)}^{\kappa_4}[(t-2\kappa_4)(N_l^2)^{t-2\kappa_4-1}(N_l^4)^{\kappa_4}D_l^2+\kappa_4(N_l^2)^{t-2\kappa_4}(N_l^4)^{\kappa_4-1}D_l^4],\\
BD(\varsigma^{even}_{t> N_u}) &= \sum_{\kappa_4=t-N_u}^{t/2} C_{N_u}^{t-2\kappa_4} C_{N_u-(t-2\kappa_4)}^{\kappa_4}[(t-2\kappa_4)(N_l^2)^{t-2\kappa_4-1}(N_l^4)^{\kappa_4}D_l^2+\kappa_4(N_l^2)^{t-2\kappa_4}(N_l^4)^{\kappa_4-1}D_l^4]\\
BD(\varsigma^{odd}_{t> N_u}) &= \sum_{\kappa_4=t-N_u}^{(t-1)/2} C_{N_u}^{t-2\kappa_4} C_{N_u-(t-2\kappa_4)}^{\kappa_4}[(t-2\kappa_4)(N_l^2)^{t-2\kappa_4-1}(N_l^4)^{\kappa_4}D_l^2+\kappa_4(N_l^2)^{t-2\kappa_4}(N_l^4)^{\kappa_4-1}D_l^4].
\end{aligned}
\tag{32}
$$

value of κ_4 ranges from zero to $t/2$. According to (19), (21), (22), the AHD of Case 1 is calculated by

$$D(\varsigma^{even}_{t\le N_u}) = \frac{1}{B}\sum_{\kappa_4=0}^{t/2} H^{all}_{(\kappa_2,\kappa_4)}. \tag{25}$$

Case 2 - t is odd with $t \le N_u$: For this case, the values of $(p_{l_1},...,p_{l_{N_u}})$ satisfying $\sum_{l=1}^{N_u} p_l = 2t$ are given by

$$
\begin{cases}
\{\underbrace{p_{l_1},\cdots,p_{l_t}}_{2\to\kappa_2=t},\underbrace{p_{l_{t+1}},\cdots,p_{l_{N_u}}}_{0\to\kappa_0=N_u-t}\},\\
\vdots\\
\{\underbrace{p_{l_1}}_{2\to\kappa_2=1},\underbrace{p_{l_2},\cdots,p_{l_{(t+1)/2}}}_{4\to\kappa_4=(t-1)/2},\underbrace{p_{l_{(t+3)/2}},\cdots,p_{l_{N_u}}}_{0\to\kappa_0=N_u-(t+1)/2}\}.
\end{cases}
\tag{26}
$$

Observe from (26) that the value of κ_4 ranges from zero to $(t-1)/2$. According to (19), (21), (22), the AHD of Case 2 is calculated by

$$D(\varsigma^{odd}_{t\le N_u}) = \frac{1}{B}\sum_{\kappa_4=0}^{(t-1)/2} H^{all}_{(\kappa_2,\kappa_4)}. \tag{27}$$

Case 3 - t is even with $t > N_u$: For this case, the values of $(p_{l_1},...,p_{l_{N_u}})$ satisfying $\sum_{l=1}^{N_u} p_l = 2t$ are given by

$$
\begin{cases}
\{\underbrace{p_{l_1},\cdots,p_{l_{t/2}}}_{4\to\kappa_4=t/2},\underbrace{p_{l_{t+1}},\cdots,p_{l_{N_u}}}_{0\to\kappa_0=N_u-t/2}\},\\
\vdots\\
\{\underbrace{p_{l_1},\cdots,p_{l_{t-N_u}}}_{4\to\kappa_4=t/2-(N_u-t/2)},\underbrace{p_{l_{(t-N_u+1)}},\cdots,p_{l_{N_u}}}_{2\to\kappa_2=2N_u-t}\}.
\end{cases}
\tag{28}
$$

Observe from (28) that the value of κ_4 ranges from $t-N_u$ to $t/2$. According to (19), (21), (22), the AHD of Case 3 is calculated by

$$D(\varsigma^{even}_{t> N_u}) = \frac{1}{B}\sum_{\kappa_4=t-N_u}^{t/2} H^{all}_{(\kappa_2,\kappa_4)}. \tag{29}$$

Case 4 - t is odd with $t > N_u$: For this case, the values of $(p_{l_1},...,p_{l_{N_u}})$ satisfying $\sum_{l=1}^{N_u} p_l = 2t$ are given by

$$
\begin{cases}
\{\underbrace{p_{l_1},\cdots,p_{l_{(t-1)/2}}}_{4\to\kappa_4=(t-1)/2},\underbrace{p_{l_{(t+1)/2}}}_{2\to\kappa_2=1}\underbrace{p_{l_{t+1}},\cdots,p_{l_{N_u}}}_{0\to\kappa_0=N_u-(t+1)/2}\},\\
\vdots\\
\{\underbrace{p_{l_1},\cdots,p_{l_{(t-N_u)}}}_{4\to\kappa_4=t-N_u},\underbrace{p_{l_{(t-N_u+1)}},\cdots,p_{l_{N_u}}}_{2\to\kappa_2=2N_u-t}\}.
\end{cases}
\tag{30}
$$

Observe from (30) that the value of κ_4 ranges from $t-N_u$ to $(t-1)/2$. According to (19), (21), (22), the AHD of Case 4 is calculated by

$$D(\varsigma^{odd}_{t> N_u}) = \frac{1}{B}\sum_{\kappa_4=t-N_u}^{(t-1)/2} H^{all}_{(\kappa_2,\kappa_4)}. \tag{31}$$

Furthermore, assuming that $N^1_{sm} = N^2_{sm} = \cdots = N^{N_u}_{sm}$ and $M_1 = M_2 = \cdots = M_{N_u}$, (25), (27), (29) and (31) can be further simplified as (32). According to (32), the closed form of the ABEP upper bound is given by (11).

IV. Capacity Analysis of Massive SM-VBLAST System

A. Capacity analysis of conventional VBLAST system

The receiver signal $\mathbf{Y}_v \in \mathbb{C}^{N_r\times 1}$ of a VBLAST system having N_t TAs and N_r RAs can be expressed as

$$\mathbf{Y}_v = \mathbf{H}\mathbf{x}_v + \mathbf{n}, \tag{33}$$

where $\mathbf{x}_v \in \mathbb{C}^{N_t\times 1}$ denotes the transmit signal, while $\mathbf{H}$ and $\mathbf{n}$ have the same definition in (4). The capacity of VBLAST can be formulated as

$$C = I(\mathbf{x_v},\mathbf{y_v}) = E\{\log_2[\det(\mathbf{I}_{N_r} + \frac{\rho}{N_t}\mathbf{H}\mathbf{H}^H)]\}, \tag{34}$$

where $\rho = 10^{\mathrm{SNR}/10}$. According to [47], the lower bound of C is expressed as

$$C \ge \mu\log_2\left[1+\frac{\rho}{N_u}\exp\left(\frac{1}{\mu}\sum_{j=1}^{\mu}\sum_{p=1}^{K-j}\frac{1}{p}-\gamma\right)\right], \tag{35}$$

where we have $\mu = \min(N_t,N_r), K = \max(N_t,N_r)$ and $\gamma \approx 0.5772$.

B. Capacity analysis of proposed massive SM-VBLAST system

In this section, the capacity of the massive SM-VBLAST system is analyzed. According to [37]-[38], the Mutual Information (MI) between the input and output signal spaces can be expressed as

$$
\begin{aligned}
I(\mathbf{x},A,\mathbf{y}) = &\underbrace{E\{\log_2[\det(\mathbf{I}_{N_r} + \frac{\rho}{N_u}\mathbf{H}_A\mathbf{H}_A^H)]\}}_{I(\mathbf{x};\mathbf{y}|A)} +\\
&\underbrace{\frac{1}{N}\sum_{i=1}^{N} E_{\mathbf{y}}\left[\log_2\frac{p(\mathbf{y}|A_i)}{p(\mathbf{y})}\right]}_{I(A;\mathbf{y})},
\end{aligned}
\tag{36}
$$

with

$$p(\mathbf{y}|A) = \frac{1}{(\pi N_0)^{N_u}}\exp\left(-\frac{\|\mathbf{y}-\mathbf{H}_A\mathbf{s}\|^2}{N_0}\right) \tag{37}$$

$$p(\mathbf{y})=\frac{1}{N}\sum_{i=1}^{N}p(\mathbf{y}|A_i). \quad (38)$$

Moreover, the lower bound of $I(\mathbf{x};\mathbf{y}|A)$ can be obtained by (35), where we have $\mu=\min(N_u,N_r), K=\max(N_u,N_r)$ and $\gamma\approx 0.5772$. In order to get the lower bound of (36), the lower bound of $I(A;\mathbf{y})$ has to be derived. According to [35], the lower bound of $I(A;\mathbf{y})$ is expressed as

$$I(A;\mathbf{y})\geq I(A;\hat{A})=\sum_{i=1}^{N}\sum_{k=1}^{N}P(A_i)P(\hat{A}_k|A_i)\log_2\frac{P(\hat{A}_k|A_i)}{P(\hat{A}_k)}, \quad (39)$$

with $N=\prod_{i=1}^{N_u}N_{sm}^{i}$ and

$$P(A_i)=\tfrac{1}{N};P(\hat{A}_k|A_i)=P(\mathbf{x}^i\to\mathbf{x}^k|M=1),$$
$$P(\hat{A}_k)=\sum_{n=1}^{N}P(\hat{A}_k|A_n)P(A_n)=\tfrac{1}{N}\sum_{n=1}^{N}P(\mathbf{x}^n\to\mathbf{x}^k|M=1), \quad (40)$$

where $P(\mathbf{x}^i\to\mathbf{x}^k|M=1)$ denotes the PEP between $\mathbf{x}^i$ and $\mathbf{x}^k$ with $M=1$, which can be computed by (9) also relying on [1]. As a result, the lower bound is expressed as

$$I^{LB}(\mathbf{x};\mathbf{y}|A)\geq\log_2\left[\det(\mathbf{I}_{N_r}+\gamma\mathbf{H}_A\mathbf{H}_A^H)\right]$$
$$+\tfrac{1}{N}\sum_{i=1}^{N}\sum_{k=1}^{N}P(\mathbf{x}^i\to\mathbf{x}^k|M=1)\log_2\frac{P(\mathbf{x}^i\to\mathbf{x}^k|M=1)}{\frac{1}{N}\sum_{n=1}^{N}P(\mathbf{x}^n\to\mathbf{x}^k|M=1)}, \quad (41)$$

where

$$P(\mathbf{x}^n\to\mathbf{x}^n|M=1)=1-\sum_{k=1,n\neq k}^{N}P(\mathbf{x}^n\to\mathbf{x}^k|M=1), \quad (42)$$

with

$$P(\mathbf{x}^n\to\mathbf{x}^k|M=1)=F(\bar{\zeta}_{M=1}). \quad (43)$$

For a massive SM-VBLAST system, the value of N is extremely large, hence the computational complexity of Eq. (41) becomes impractical. According to [1], there are some common values of $P(\mathbf{x}^n\to\mathbf{x}^k|M=1)$ for different n and k, so that (41) can be further simplified, which is introduced as follows.

For the case of $M=1$, the activated TAC transmits all symbols $'1'$, so that we have

$$\|\mathbf{x}_l^n-\mathbf{x}_l^k\|^2=p_l=\begin{cases}0, & \text{if } \mathbf{x}_l^n=\mathbf{x}_l^k\\ 2, & \text{if } \mathbf{x}_l^n\neq\mathbf{x}_l^k\end{cases},\ l=1,\cdots N_u. \quad (44)$$

The number of $p_l=0$ and $p_l=2$ can be expressed as

$$N_l^0=1,N_l^2=2^{B_l}-1,l=(1,...,N_u). \quad (45)$$

According to (15), the value of $\bar{\zeta}_{t|M=1}$ is expressed as

$$\bar{\zeta}_{t|M=1}=\frac{\left\|\mathbf{x}^n-\mathbf{x}^k\right\|^2}{2\sigma^2}=\frac{t}{\sigma^2}, \quad (46)$$

where t is the number of nonzero elements in $(p_1,p_2,p_3,...,p_{N_u})$ for this case. As a result, there are a total of N_u different values of $F(\bar{\zeta}_{M=1})$ as $F(\bar{\zeta}_{1|M=1}),F(\bar{\zeta}_{2|M=1}),...,F(\bar{\zeta}_{t|M=1}),...,F(\bar{\zeta}_{N_u|M=1})$. For each value of $F(\bar{\zeta}_{t|M=1})$, the t nonzero values can be expressed as $(p_{l_1}=...=p_{l_t}=2)$. More specifically, we have $(l_1,l_2,...,l_t)\in I_{N_u}^t$, which indicates that the ICS consists of t indices selected from $(1,2,...,N_u)$. For a certain combination of $(l_1,l_2,...,l_t)$, there are a total of $\prod_{i=1}^{t}N_{l_i}^2$ cases to satisfy $(p_{l_1}=...=p_{l_t}=2)$. As a result, for a given value of $\mathbf{x}^n$, the total number φ_t of $\mathbf{x}^k$ having the value of $\bar{\zeta}_{t|M=1}$ is expressed as

$$\varphi_t=\begin{cases}C_{N_u}^t\left(2^{B_1}-1\right)^t, \text{if} B_1=\cdots=B_{N_u}\\ \sum_{(l_1,...,l_t)\in I_{N_u}^t}\prod_{i=1}^{t}N_{l_i}^2=\sum_{(l_1,...,l_t)\in I_{N_u}^t}\prod_{i=1}^{t}\left(2^{B_{l_i}}-1\right). \text{else}\end{cases} \quad (47)$$

Since (47) satisfies

$$\sum_{t=1}^{N_u}\varphi_t=\sum_{t=1}^{N_u}\sum_{(l_1,...,l_t)\in I_{N_u}^t}\prod_{i=1}^{t}\left(2^{B_{l_i}}-1\right)=N-1, \quad (48)$$

which is proved in Appendix, the value of $\sum_{k=1,k\neq m}^{N}P(\mathbf{x}^m\to\mathbf{x}^k|M=1)$ is expressed as

$$\sum_{k=1,k\neq m}^{N}P(\mathbf{x}^m\to\mathbf{x}^k|M=1)=\sum_{t=1}^{N_u}\varphi_t F\left(\frac{t}{\sigma^2}\right), \quad (49)$$

and the value of $P(\mathbf{x}^m\to\mathbf{x}^m|M=1)$ is expressed as

$$P(\mathbf{x}^m\to\mathbf{x}^m|M=1)=1-\sum_{t=1}^{N_u}\varphi_t F\left(\frac{t}{\sigma^2}\right). \quad (50)$$

As a result, the lower bound of $I(A;\mathbf{y})$ is simplified as

$$\begin{aligned}&\tfrac{1}{N}\sum_{i=1}^{N}\sum_{k=1}^{N}P(\mathbf{x}^i\to\mathbf{x}^k|M=1)\log_2\frac{P(\mathbf{x}^i\to\mathbf{x}^k|M=1)}{\frac{1}{N}\sum_{m=1}^{N}P(\mathbf{x}^m\to\mathbf{x}^k|M=1)}\\ &=\tfrac{1}{N}\sum_{i=1}^{N}\Bigg\{\sum_{k\neq i}P(\mathbf{x}^i\to\mathbf{x}^k|M=1)\log_2\left[NP(\mathbf{x}^i\to\mathbf{x}^k|M=1)\right]\\ &+\sum_{k=i}P(\mathbf{x}^i\to\mathbf{x}^k|M=1)\log_2\left[NP(\mathbf{x}^i\to\mathbf{x}^k|M=1)\right]\Bigg\}\\ &=\tfrac{1}{N}\sum_{i=1}^{N}\Bigg\{\sum_{t=1}^{N_u}\varphi_t F(\tfrac{t}{\sigma^2})\log_2\left[NF(\tfrac{t}{\sigma^2})\right]\\ &+[1-\sum_{t=1}^{N_u}\varphi_t F(\tfrac{t}{\sigma^2})]\log_2\{N[1-\sum_{t=1}^{N_u}\varphi_t F(\tfrac{t}{\sigma^2})]\}\Bigg\}\\ &=\sum_{t=1}^{N_u}\varphi_t F(\tfrac{t}{\sigma^2})\log_2\left[NF(\tfrac{t}{\sigma^2})\right]\\ &+[1-\sum_{t=1}^{N_u}\varphi_t F(\tfrac{t}{\sigma^2})]\log_2\{N[1-\sum_{t=1}^{N_u}\varphi_t F(\tfrac{t}{\sigma^2})]\}.\end{aligned} \quad (51)$$

According to (36), (39), (41) and (51), the closed form of the massive SM-VBLAST system capacity lower bound becomes

$$\begin{aligned}I^{LB}(\mathbf{x};\mathbf{y}|A)&\geq\mu\log_2[1+\tfrac{\rho}{N_u}\exp(\tfrac{1}{\mu}\sum_{j=1}^{\mu}\sum_{p=1}^{K-j}\tfrac{1}{p}-\gamma)]\\ &+[1-\sum_{t=1}^{N_u}\varphi_t F(\tfrac{t}{\sigma^2})]\log_2\{N[1-\sum_{t=1}^{N_u}\varphi_t F(\tfrac{t}{\sigma^2})]\}\\ &+\sum_{t=1}^{N_u}\varphi_t F(\tfrac{t}{\sigma^2})\log_2[NF(\tfrac{t}{\sigma^2})].\end{aligned} \quad (52)$$

where φ_t and $F(\frac{t}{\sigma^2})$ can obtained by (47) and (9), respectively.

V. Efficient ECM assisted Compressive Sensing Detector for Massive SM-VBLAST System

In this section, an efficient ECM assisted CS detector is designed for massive SM-VBLAST systems, which is shown in Fig. 2. A threshold is designed to judge whether

Algorithm 2 The proposed ECM-CS detector for the Massive SM-VBLAST system

Input: $\hat{\mathbf{y}}$, $\hat{\mathbf{H}}$;
Output: $\mathbf{x}_o$.

Obtain $\hat{\mathbf{x}}^0$ by conventional CS algorithm and get the initial $\mathbf{R}^0 = \left\|\mathbf{y} - \mathbf{H}\hat{\mathbf{x}}^0\right\|^2$.
if $\mathbf{R}^0 \le V_{\text{th}}$ **then**
  $\mathbf{x}_o = \hat{\mathbf{x}}^0$, return;
else
  for $t \in (1, N_{\text{iter}})$ **do**
    $\hat{\mathbf{x}}^t$=$\hat{\mathbf{x}}^{t-1}$,$\mathbf{R}^t = \mathbf{R}^{t-1}$,$\tilde{\mathbf{R}}^t = \phi$;
    for $l \in (1, N_u)$ **do**
      Remove the l-th symbol from $\hat{\mathbf{x}}^t$ as $\hat{\mathbf{x}}^{l,t} = (\hat{\mathbf{x}}_1^t, \cdots, \hat{\mathbf{x}}_{l-1}^t, \mathbf{O}_{N_{sm}^l}, \hat{\mathbf{x}}_{l+1}^t \cdots, \hat{\mathbf{x}}_{N_u}^t)^T$;
      Get the residual vector $\mathbf{R}^{l,t}$ by (54);
      $[L_o, v] = \arg sort(|\mathbf{H}^H \mathbf{R}^{l,t}|,' desender')$;
      Get the first m indices as $\mathcal{I}_m = L_o(1:m)$;
      Re-estimate the l-th symbol $\tilde{\mathbf{x}}_l^t$ as $(\tilde{k}_l, \tilde{s}_l) = \underset{k_l \in \mathcal{I}_m, s_l \in \mathcal{S}}{\arg\min} \left\|\mathbf{R}^{l,t} - \mathbf{h}_{k_l} s_l\right\|^2$;
      Obtain the estimated signal $\tilde{\mathbf{x}}^{l,t} = (\hat{\mathbf{x}}_1^t, \cdots, \hat{\mathbf{x}}_{l-1}^t, \tilde{\mathbf{x}}_l^t, \hat{\mathbf{x}}_{l+1}^t \cdots, \hat{\mathbf{x}}_{N_u}^t)^T$;
      Update the l-th residual vector as $\tilde{\mathbf{R}}^{l,t} = \mathbf{y} - \mathbf{H}\tilde{\mathbf{x}}^{l,t} = \mathbf{R}^{l,t} - \mathbf{h}_{\tilde{k}_l}\tilde{s}_l$;
      if $\|\tilde{\mathbf{R}}^{l,t}\|^2 \le V_{\text{th}}$ **then**
        $\mathbf{x}_o = \tilde{\mathbf{x}}^{l,t}$, return;
      else
        $\tilde{\mathbf{R}}^t = [\tilde{\mathbf{R}}^t, \tilde{\mathbf{R}}^{l,t}]$;
      end if
    end for
    $\|\tilde{\mathbf{R}}_{\min}^t\|^2 = \min_{\forall l}(\|\tilde{\mathbf{R}}^{l,t}\|^2)$ and get its corresponding estimated signal $\tilde{\mathbf{x}}^{l_{\min},t}$;
    if $\|\tilde{\mathbf{R}}_{\min}^t\|^2 = \|\mathbf{R}^t\|^2$ **then**
      $\mathbf{x}_o = \tilde{\mathbf{x}}^{l_{\min},t}$, return;
    else
      Update the signal and residual vector as $\hat{\mathbf{x}}^t = \tilde{\mathbf{x}}^{l_{\min},t}$, $\mathbf{R}^t = \tilde{\mathbf{R}}_{\min}^t$;
    end if
  end for
  $\mathbf{x}_o = \tilde{\mathbf{x}}^{l_{\min},N_{\text{iter}}}$.
end if

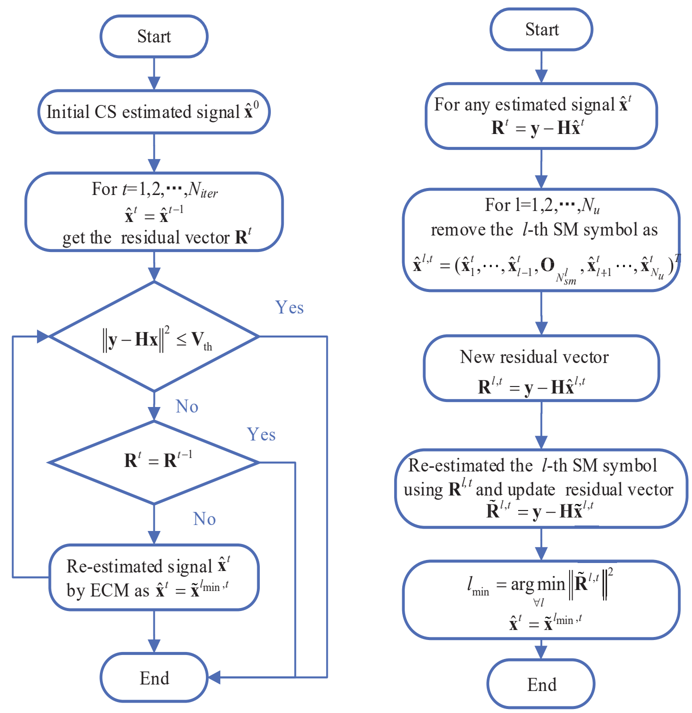

(a) The process of ECM-CS detector

(b) The process of ECM algorithm

Fig. 2. The process of our proposed ECM-CS detector and ECM algorithm.

the initial signal estimated by the conventional CS algorithm is reliable or unreliable. If it is judged to be unreliable, our ECM means is invoked to further test the estimated signal's reliability. We will show that this ECM technique is also capable of correcting the erroneous indices.

A. Proposed Detector

Step 1: As shown in Fig. 2(a), we first obtain the initial transmit signal $\hat{\mathbf{x}}^0 = (\hat{\mathbf{x}}_1^0, \cdots, \hat{\mathbf{x}}_l^0, \cdots, \hat{\mathbf{x}}_{N_u}^0)^T$ via the conventional CS algorithm.

Step 2: Determine wether the estimated signal is reliable or unreliable. If the ED of the estimated signal $(\Lambda, \mathbf{s})$ satisfies

$$\left\|\mathbf{y} - \mathbf{H}\hat{\mathbf{x}}^0\right\|^2 \le V_{\text{th}}, \tag{53}$$

where $V_{\text{th}} = \beta N_r \sigma^2$, then $(\Lambda, \mathbf{s})$ is deemed to be the final detection result with β being a constant. The choice of β is analyzed in the threshold design part of Section V-B.

Step 3: Otherwise, the result $\hat{\mathbf{x}}^0$ will be further judged to be either reliable or unreliable by our proposed ECM scheme. For the reliable result $\hat{\mathbf{x}}^0$, it will be judged as the final result by calculating about $N_u mM$ EDs, where m is a preset number to strike a performance vs. complexity trade-off. By contrast, for the unreliable result $\hat{\mathbf{x}}^0$, it will be corrected by calculating about $n_e N_u mM$ EDs, where n_e represents the number of errors that our ECM can correct.

B. Proposed ECM Scheme

In the proposed ECM scheme, the l-th symbol $l = (1, ..., N_u)$ $\hat{\mathbf{x}}_l^0$ of the initial result $\hat{\mathbf{x}}^0$ will be further judged to be either reliable or unreliable in the sequel. The total number of checking iterations is dominated by the value of n_e. Assuming that the t-th iteration result is $\hat{\mathbf{x}}^t = (\hat{\mathbf{x}}_1^t, \cdots, \hat{\mathbf{x}}_l^t, \cdots, \hat{\mathbf{x}}_{N_u}^t)^T$ associated with TAC index $\hat{\Lambda} = (\hat{k}_1, ..., \hat{k}_{N_u})$ and symbol vector $\hat{\mathbf{s}} = (\hat{s}_1, ..., \hat{s}_{N_u})$, the ECM operates as follows.

Step 1: As shown in Fig. 2(b), we first remove the l-th symbol $\hat{\mathbf{x}}_l$ from $\hat{\mathbf{x}}^t$ as $\hat{\mathbf{x}}^{l,t} = \hat{\mathbf{x}}^t \backslash \hat{\mathbf{x}}_l^t = (\hat{\mathbf{x}}_1^t, \cdots, \hat{\mathbf{x}}_{l-1}^t, \mathbf{O}_{N_{sm}^l}, \hat{\mathbf{x}}_{l+1}^t \cdots, \hat{\mathbf{x}}_{N_u}^t)^T$, where $\mathbf{O}_{N_{sm}^l}$ denotes N_{sm}^l zeros. Assuming that $\Lambda = (k_1, ..., k_{N_u}), \mathbf{s} = (s_1, ..., s_{N_u})$ are the accurate TAC index and symbol vector, two residual vectors in the t-th iteration are defined as

$$\begin{aligned}\mathbf{R}^t &= \mathbf{y} - \mathbf{H}\hat{\mathbf{x}}^t = \mathbf{R}_1^t + \dots \mathbf{R}_{l-1}^t + \mathbf{R}_l^t + \mathbf{R}_{l+1}^t + \dots + \mathbf{R}_{N_u}^t,\\ \mathbf{R}^{l,t} &= \mathbf{y} - \mathbf{H}\hat{\mathbf{x}}^{l,t} = \mathbf{R}_1^t + \dots \mathbf{R}_{l-1}^t + \mathbf{h}_{k_l} s_l + \mathbf{R}_{l+1}^t + \dots + \mathbf{R}_{N_u}^t,\end{aligned} \tag{54}$$

where $\mathbf{R}_l^t = \mathbf{h}_{k_l} s_l - \mathbf{h}_{\hat{k}_l} \hat{s}_l$.

Step 2: Re-estimate the l-th symbol as $\tilde{\mathbf{x}}_l^t$ based on the Multipath Matching Pursuit (MMP) algorithm [44]. Specifically, the new index $\tilde{k}_l$ and symbol $\tilde{s}_l$ of the signal $\tilde{\mathbf{x}}_l^t$ can be estimated by

$$(\tilde{k}_l, \tilde{s}_l) = \underset{k_l \in \mathcal{I}_m, s_l \in \mathcal{S}}{\arg\min} \left\| \mathbf{R}^{l,t} - \mathbf{h}_{k_l} s_l \right\|^2, \tag{55}$$

where $\mathcal{S}$ is the set of APM symbols and $\mathcal{I}_m$ denotes the m-th possible candidates, which is obtained by

$$\begin{aligned}&[L_o, v] = \arg sort(|\mathbf{H}_{[N_{sm}^l]}^H \mathbf{R}^{l,t}|, 'desender'),\\ &\mathcal{I}_m = L_o(1:m).\end{aligned} \tag{56}$$

where $\mathbf{H}_{[N_{sm}^l]}^H$ denotes the N_{sm}^l rows of $\mathbf{H}^H$ corresponding to the l-th symbol $\mathbf{x}_l$.

Step 3: Update the estimated symbol as $\tilde{\mathbf{x}}^{l,t} = (\hat{\mathbf{x}}_1^t, \cdots, \hat{\mathbf{x}}_{l-1}^t, \tilde{\mathbf{x}}_l^t, \hat{\mathbf{x}}_{l+1}^t \cdots, \hat{\mathbf{x}}_{N_u}^t)^T$.

Step 4: Update the residual vector based on the estimated result $\tilde{\mathbf{x}}^{l,t}$ as

$$\tilde{\mathbf{R}}^{l,t} = \mathbf{y} - \mathbf{H}\tilde{\mathbf{x}}^{l,t} = \mathbf{R}^{l,t} - \mathbf{h}_{\tilde{k}_l} \tilde{s}_l. \tag{57}$$

Step 5: Repeat Steps 1-4 and obtain N_u residual vectors $\tilde{\mathbf{R}}^t = [\tilde{\mathbf{R}}^{1,t}, ..., \tilde{\mathbf{R}}^{l,t}, ..., \tilde{\mathbf{R}}^{N_u,t}]$. Then find the minimum value of $\|\tilde{\mathbf{R}}^t\|^2$ as $\|\tilde{\mathbf{R}}_{\min}^t\|^2$.

Step 6: Judge the estimated result $\hat{\mathbf{x}}^t$ to be reliable or unreliable using $\tilde{\mathbf{R}}_{\min}^t$. Specifically, if we have

$$\|\tilde{\mathbf{R}}_{\min}^t\|^2 = \|\mathbf{R}^t\|^2, \tag{58}$$

it implies that there is no erroneous result in $\hat{\mathbf{x}}^t$ and it will be considered as the final result. If we have

$$\|\tilde{\mathbf{R}}_{\min}^t\|^2 < \mathbf{R}^t \text{ and } \|\tilde{\mathbf{R}}_{\min}^t\|^2 < V_{\text{th}}, \tag{59}$$

it means that there is only one erroneous result in $\hat{\mathbf{x}}^t$ and it will be corrected in this step. Then the updated transmit signal $\tilde{\mathbf{x}}^{l_{\min},t}$ having the ED of $\|\tilde{\mathbf{R}}_{\min}^t\|^2$ is considered as the final result. Otherwise, there may be more than one erroneous result in $\hat{\mathbf{x}}^t$ and the checking process will be continued. The updated transmit signal $\tilde{\mathbf{x}}^{l_{\min},t}$ will be considered as the initial result of the $(t+1)$-th iteration.

In conclusion, the proposed detector is summarized at a glance in **Algorithm 2**, where N_{iter} means the number of iteration, which is usually smaller than N_u.

C. Complexity Analysis

In this subsection, the complexity of the proposed detector designed for the massive SM-VBLAST system is analyzed in terms of the number of real-valued multiplications and additions [40]. For specific matrices $\mathbf{A} \in \mathbb{C}^{m \times n}$, $\mathbf{B} \in \mathbb{C}^{n \times p}$, $\mathbf{c} \in \mathbb{C}^{n \times 1}$ and $\mathbf{d} \in \mathbb{C}^{n \times 1}$, the operations of $\mathbf{AB}$, $\|\mathbf{c}\|_F^2$ and $\mathbf{c} \pm \mathbf{d}$ require $8mnp - 2mp$, $4n - 1$, and $2n$ flops, respectively. According to (54)-(57), the complexity of the proposed detector can be expressed as

$$\begin{aligned}C_P = C_{CS} &+ \underbrace{8N_u N_r (N_u - 1)}_{\text{Complexity of (54)}} N_{avg}^e + \underbrace{N_{avg}^e \sum_{l=1}^{N_u} 8 N_t N_{sm}^l}_{\text{Complexity of (56)}} +\\ &\underbrace{10 N_u N_r m M N_{avg}^e}_{\text{Complexity of (55)}} + \underbrace{10 N_u N_r N_{avg}^e}_{\text{Complexity of (57)}},\end{aligned} \tag{60}$$

where C_{CS} denotes the complexity of the conventional CS detector and N_{avg}^e denotes the average number of errors the ECM has corrected, which is smaller than N_u. In order to strike a performance vs. complexity trade-off, we opted for low complexity CS algorithms such as CoSaMP and OMP in the first step, whose complexity is expressed as:

$$\begin{aligned}&C_{\text{Cosamp}} = (12N_r - 1 + 8N_r N_t + 2N_t + 4K^3 +\\ &12 N_r K^2 + 7K^2 + 6 N_r K)\omega_{\text{Co}},\\ &C_{OMP} = N_u (8 N_r N_t + 10 N_r N_{sm}^l M).\end{aligned} \tag{61}$$

where $K = 3N_u$ and ω_{Co} denote the average iterations in the CosaMP algorithm.

D. Performance Analysis for Our Proposed ECM assisted CS Detector

In this section, the performance of the proposed detector is analyzed. According to Algorithm 2, the BER performance of the proposed detector can be characterized as

$$P_e^{\text{pro.}} \approx 1 - \underbrace{(1 - P(\rho_e \leq V_{\text{th}}))}_{\text{Eq.(53)}} \underbrace{(1 - P_e^{\text{ECM}})}_{\text{Eq.(55)}} \underbrace{(1 - P_e^{\text{ML}})}_{\text{Eq.(59)}}, \tag{62}$$

where P_e^{ML}, $P(\rho_e \leq V_{\text{th}})$ and P_e^{ECM} denote the error probability estimated by the ML detector of (59), by the threshold based decision of (53) and by the ECM detector of (55). For a given antenna configuration, the values of P_e^{ML} are fixed. As a result, the performance of the proposed detector is mainly dominated by $P(\rho_e \leq V_{\text{th}})$ and P_e^{ECM}, which will be analyzed in detail as follows.

1) Threshold Design

According to [40], the ED between the estimated signal $\hat{\mathbf{x}}$ and the receiver signal is expressed as

$$\begin{cases} \rho = \|\mathbf{y} - \mathbf{H}\hat{\mathbf{x}}\|^2 = \|\mathbf{n}\|^2, \text{if } \hat{\mathbf{x}} = \mathbf{x},\\ \rho_e = \|\mathbf{y} - \mathbf{H}\hat{\mathbf{x}}\|^2 = \|\mathbf{H}(\mathbf{x} - \hat{\mathbf{x}}) + \mathbf{n}\|^2, \text{if } \hat{\mathbf{x}} \neq \mathbf{x}.\end{cases} \tag{63}$$

According to [40], both $\frac{2\rho}{\sigma^2}$ and $\frac{2\rho_e}{\sigma^2 + ||\mathbf{x} - \hat{\mathbf{x}}||^2}$ follow the Chi-square distribution with degree $2N_r$ as

$$\frac{2\rho}{\sigma^2} \sim \chi^2(2N_r), \frac{2\rho_e}{\sigma^2 + ||\mathbf{x} - \hat{\mathbf{x}}||^2} \sim \chi^2(2N_r), \tag{64}$$

whose Probability Density Function (PDF) is given by

$$f_{\chi^2(2N_r)}(x) = \begin{cases} \frac{1}{2^{N_r}\Gamma(N_r)} e^{-x/2} x^{N_r - 1}, x > 0\\ 0, \qquad x \leqslant 0 \end{cases}. \tag{65}$$

As a result, the values of $P(\rho \leq V_{\text{th}})$ and $P(\rho_e \leq V_{\text{th}})$ can be obtained by

$$P(\rho \leq V_{\text{th}}) = \int_0^{\frac{2V_{\text{th}}}{\sigma^2}} f_{\chi^2(2N_r)}(x) dx, \tag{66}$$

$$P(\rho_e \leq V_{\text{th}}) = \int_0^{\frac{2V_{\text{th}}}{\sigma^2 + ||\mathbf{x} - \hat{\mathbf{x}}||^2}} f_{\chi^2(2N_r)}(x) dx. \tag{67}$$

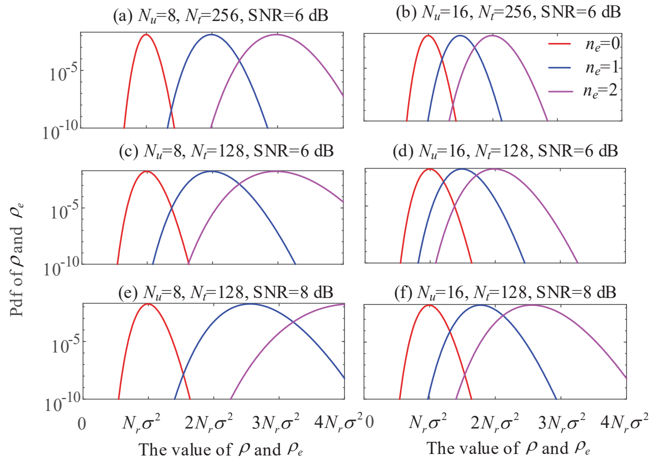

Fig. 3. PDF of ρ and ρ_e with different antenna setups, which are calculated by (65).

TABLE II
V_{TH} DESIGN FOR SPECIFIC SETUPS.

(N_t, N_u, N_r, M)	V_{th}
$(128, 16, 64, 4)$	$N_r\sigma^2$
$(128, 16, 128, 4)$	$0.925N_r\sigma^2$
$(120, 30, 128, 4)$	$0.91N_r\sigma^2$
$(160, 40, 128, 4)$	$0.91N_r\sigma^2$
$(240, 60, 256, 4)$	$0.89N_r\sigma^2$
$(320, 80, 256, 4)$	$0.89N_r\sigma^2$

Assuming that $\rho_e^{n_e}$ represents the ED with n_e errors in the estimated signal $\hat{\mathbf{x}}$, Fig. 3 portrays the PDF of ρ and ρ_e associated with different setups at 6 dB and 8 dB, respectively. It is clear that the PDFs of ρ and ρ_e are associated with specific setups and SNRs. If the threshold V_{th} is set too small, even the most reliable signal will be judged to be unreliable, which may impose extra search complexity. By contrast, if the threshold V_{th} is set too high, even an unreliable signal having one or two errors will also be judged to be reliable, which may result in erroneous detection. In this paper, the thresholds are set based on the ABEP, where the value of ρ_e is close to the theoretical ML detector's performance. Based on this design principle, the thresholds for the specific setups are presented in Table II.

2) Error Correction Mechanism

In this section, the performance of the ECM scheme has been analyzed.

Case 1 - $n_e = 0$**:** If the ED of the signal that was deemed reliable does not satisfy (53), then it will be judged to be reliable by the ECM of (58). Specifically, after removing the l-th symbol $\hat{\mathbf{x}}_l$, the residual vector in (54) can be updated as $\tilde{\mathbf{R}}^{l,t} = \mathbf{h}_{k_l} s_l + \mathbf{n}$. Assuming that no errors are encountered by (55), the new estimated index and symbol are $\hat{k}_l = k_l$ and $\hat{s}_l = s_l$. Then we will have $\tilde{\mathbf{R}}^{1,t} = ... = \tilde{\mathbf{R}}^{l,t} = ... = \tilde{\mathbf{R}}^{N_u,t}$. As a result, the estimated signal will ultimately be judged to be reliable by (58).

Case 2 - $n_e = 1$**:** Assuming that only the l-th index and symbol are estimated inaccurately as $\hat{k}_l$ and $\hat{s}_l$, according to (63), the ED ρ_e^1 is expressed as

$$\rho_e^1 = \left\| h_{k_l} s_{k_l} - h_{k_{\hat{k}_l}} \hat{s}_l + \mathbf{n} \right\|^2 . \tag{68}$$

For the l-th step, after removing the l-th symbol $\hat{\mathbf{x}}_l$, the residual vector is updated as $\tilde{\mathbf{R}}^{l,t} = \mathbf{h}_{k_l} s_l + \mathbf{n}$. Assuming that no errors are encountered by (55), k_l and s_{k_l} can be estimated accurately and the ED is updated as $\|\tilde{\mathbf{R}}^t_{\min}\|^2 = \rho = \|\mathbf{n}\|^2$. If $\|\tilde{\mathbf{R}}^t_{\min}\|^2 < \rho_e^1$, this erroneous index can be corrected by this ECM. Otherwise, the error probability is the same as that of the ML detector.

Case 3 - $n_e \geq 1$**:** Assuming that the unreliable indices are $\hat{k}_{l_1}, ..., \hat{k}_{l_{n_e}}$, the ED between the estimated signal and the received signal is expressed as

$$\begin{aligned} \rho_e^2 &= \|h_{k_{l_1}} s_{k_{l_1}} - h_{\hat{k}_{l_1}} \hat{s}_{k_{l_1}} + h_{k_{l_2}} s_{k_{l_2}} - h_{\hat{k}_{l_2}} \hat{s}_{k_{l_2}}\|^2, \\ &\vdots \\ \rho_e^{n_e} &= \|h_{k_{l_1}} s_{k_{l_1}} - h_{\hat{k}_{l_1}} \hat{s}_{k_{l_1}} + \cdots h_{k_{l_{n_e}}} s_{k_{l_{n_e}}} - h_{\hat{k}_{l_{n_e}}} \hat{s}_{k_{l_{n_e}}}\|^2. \end{aligned} \tag{69}$$

If $\rho_e^{n_e-1} < \rho_e^{n_e}$ holds true, the ECM becomes capable of correcting the erroneous indices. Fig. 4 portrays the erroneous decision probabilities $P_e(\rho_e^{n_e-1} < \rho_e^{n_e})$ of $\rho_e^{n_e-1} < \rho_e^{n_e}$ in conjunction with $N_r = 128$ and 256 antennas. Fig. 4 shows that $P_e(\rho \leq \rho_e^1) < P_e(\rho_e^1 \leq \rho_e^2) < P_e(\rho_e^2 \leq \rho_e^3) < P_e(\rho_e^3 \leq \rho_e^4)$ holds true for these setups. Moreover, these values monotonically decrease both with N_r and the SNR. This implies that the proposed ECM works better for larger values of N_r in the high SNR regions. However, when the MMP detector of (55) encounters estimation errors, the proposed ECM may suffer from error propagation.

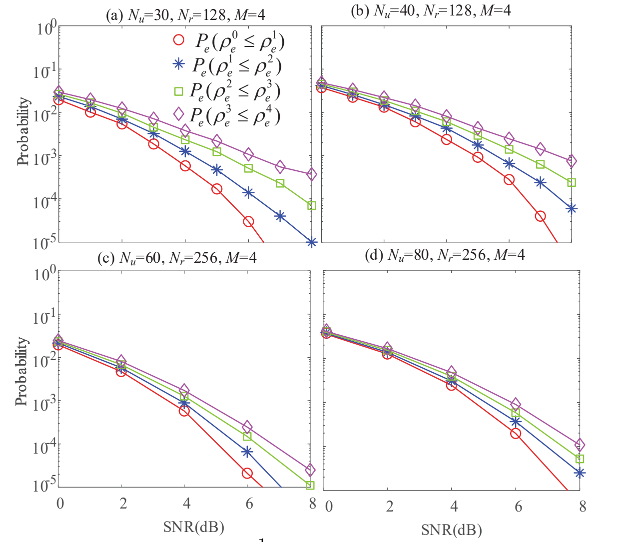

Fig. 4. The value of $P_e(\rho_e^{n_e-1} \leq \rho_e^{n_e})$ with different setups obtained by simulation results.

VI. Simulation Results

In this section, the capacity, the BER performance and complexity of the massive SM-VBLAST system are analyzed in conjunction with different antenna configurations. For P2P communication, the Largest Number First (LNF) principle of [1] is employed[2]. For UL communication, the

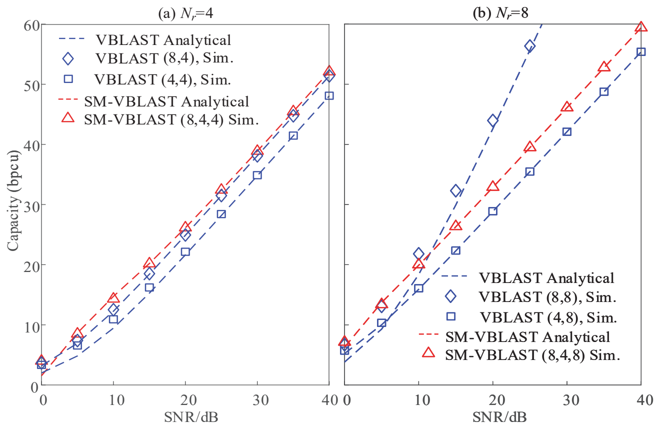

Fig. 5. Comparison of the capacity for different antenna configurations. The simulated and analytical capacity of VBLAST is calculated by the Monte-Carlo simulation of (34) and from the analytical lower bound in (35), respectively. The simulated and analytical capacity of SM-VBLAST is calculated by the Monte-Carlo simulation of (36) and from the analytical lower bound in (52), respectively.

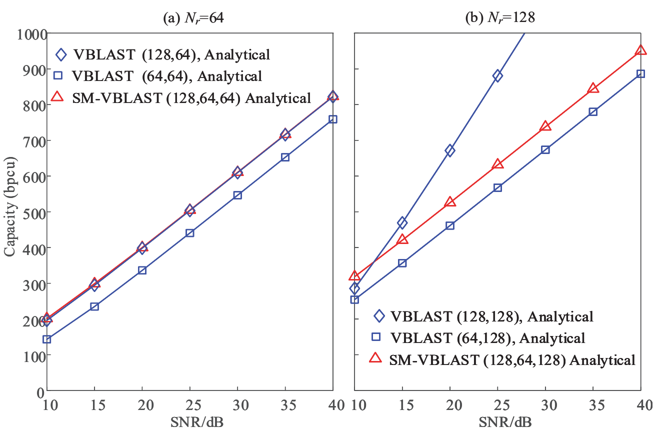

Fig. 6. Comparisons of the analytical capacity of the massive SM-VBLAST system and of the VBLAST system, which are calculated by (35) and (52), respectively.

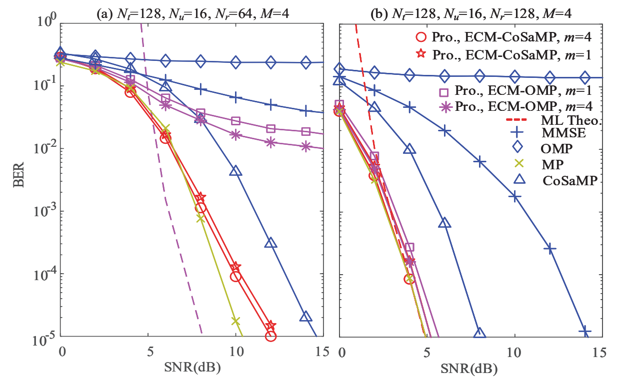

Fig. 7. Performance comparison with different CS detectors for SM-VBLAST systems at 80 bpcu. a) $N_t = 128, N_u = 16, N_r = 64$, $M = 4$; b) $N_t = 128, N_u = 16, N_r = 128$, $M = 4$. These systems can also be considered as UL systems with 16 users. Each user is equipped with 8 antennas.

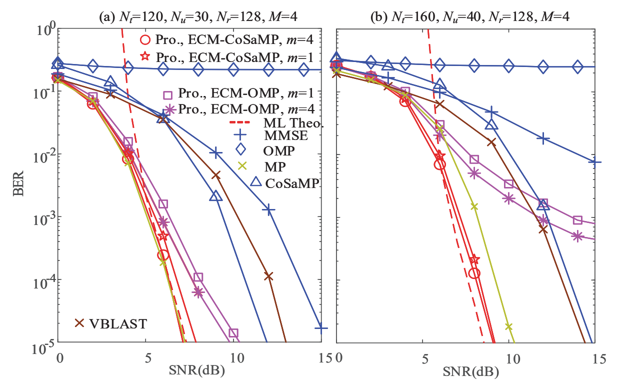

Fig. 8. Performance comparison with different CS detectors for SM-VBLAST systems. a) $N_t = 120, N_u = 30, N_r = 128$, $M = 4$ at 120 bpcu; b) $N_t = 160, N_u = 40, N_r = 128$, $M = 4$ at 160 bpcu. These systems can also be considered as UL systems with 30 and 40 users. Each user is equipped with 4 antennas.

notations can be found in Table I.

A. Capacity Analysis Results

Figs. 5-6 portray the maximum achievable rate of the SM-VBLAST systems having different number of RAs. In order to achieve the maximum attainable rate, $N_u = N_t/2$ is employed in SM-VBLAST. The capacity of the classic VBLAST systems having the same number of RF chains and TAs are added as benchmarkers. In order to evaluate our analytical lower bound, the capacity of SM-VBLAST is calculated by Monte-Carlo simulation and analytical result are compared using small-scale MIMO setups in Fig. 5. Specifically, $(N_t, N_u, N_r) = (8, 4, 4), (8, 4, 8)$ are employed for SM-VBLAST, while $(N_t, N_r) = (8, 4), (4, 4), (8, 8), (4, 8)$ are used for VBLAST system. Observe from Fig. 5 that the Monte-Carlo results closely approach the analytical lower bound upon increasing the SNR values.

Furthermore, in the massive setups of Fig. 6, the capacity calculation based on the Monte-Carlo simulation of (36) becomes impractical, hence only the analytical lower bound of (52) is included for comparison. Observe from Figs.5-6 that since the antenna indices are activated for conveying extra information, the capacity of the SM-VBLAST system is always higher than that of the VBLAST system having the same number of RF chains and RAs. When comparing it to the VBLAST system having the same values of N_t, N_r, the proposed SM-VBLAST is capable of approaching the MIMO capacity in the context of the under-determined antenna configuration, while it is still far from the MIMO capacity in the context of the over-determined antenna configuration. This implies that an enhanced SM-VBLAST system can be developed for approaching the MIMO capacity for the balanced antenna setup, which will be considered in our future work.

[2]**LNF based Principle:** In the t-th $t \in (2, ..., N_u\text{-}1)$ step, the largest number N^L_{t-1} in the $(t-1)$-th set $\mathcal{N}_{t-1}$ is decomposed into two equal numbers as $(N^L_{t-1}/2, N^L_{t-1}/2)$, where $\mathcal{N}_1 = [N_t]$. As a result, the decomposed set in the t-th step can be expressed as $\mathcal{N}_t = (\mathcal{N}_{t-1} \backslash N^L_{t-1}, N^L_{t-1}/2, N^L_{t-1}/2)$. These processes continue, until we get N_u values as $N^1_{sm}, ..., N^{N_u}_{sm}$.

TABLE III
COMPLEXITY COMPARISON OF THE PROPOSED ECM-OMP, ECM-COSAMP AND MP DETECTORS.

(N_t, N_u, N_r, M) SNR	scheme	N^e_{avg}	Complexity normalized by the MP detector
$(128, 16, 64, 4)$ 10 dB	Pro.ECM-OMP $m = 4$	11.8	3.1%
	Pro.ECM-CoSaMP $m = 4$	1.1	4.7%
$(128, 16, 128, 4)$ 6 dB	Pro.ECM-OMP $m = 4$	8.6	1.25%
	Pro.ECM-CoSaMP $m = 4$	1.02	2.44%
$(120, 30, 128, 4)$ 8 dB	Pro.ECM-OMP $m = 4$	18.7	4.55%
	Pro.ECM-CoSaMP $m = 4$	1.4	8.36%
$(160, 40, 128, 4)$ 10 dB	Pro.ECM-OMP $m = 4$	29.6	7.64%
	Pro.ECM-CoSaMP $m = 4$	1.94	10.85%
$(240, 60, 256, 4)$ 8 dB	Pro.ECM-OMP $m = 4$	36.5	6.54%
	Pro.ECM-CoSaMP $m = 4$	1.95	8.25%
$(320, 80, 256, 4)$ 8 dB	Pro.ECM-OMP $m = 4$	58.4	11.65%
	Pro.ECM-CoSaMP $m = 4$	8.84	11.92%

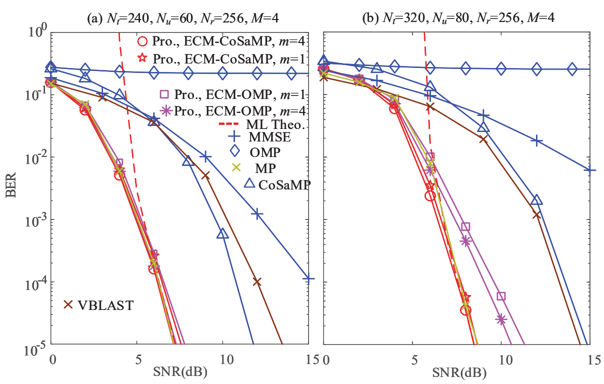

Fig. 9. Performance comparison with different CS detectors for SM-VBLAST systems. a) $N_t = 240, N_u = 60, N_r = 256$, $M = 4$ at 240 bpcu; b) $N_t = 320, N_u = 80, N_r = 256$, $M = 4$ at 320 bpcu. These systems can also be considered as UL systems with 60 and 80 users. Each user is equipped with 4 antennas.

B. BER Performance Results

In this section, the BERs of different CS SM-VBLAST detectors are compared for different antenna configurations. The optimal thresholds are selected based on Table II. The theoretical ABEPs of ML detectors are calculated by (32). Moreover, both the OMP and CoSaMP detectors have been employed in our proposed detector for comparison, called ECM-OMP and ECM-CoSaMP detectors, respectively. QPSK is employed for massive SM-VBLAST in these simulation results.

Fig. 7 compares the performances of different detectors for massive SM-VBLAST systems having (N_t, N_u, N_r)=(128,16,64) and (128,16,128), respectively. Observe from Fig. 7 that the performances of the proposed ECM-CoSaMP and ECM-OMP detectors are improved as m increases and they outperform the conventional OMP as well as CosaMP and MMSE detectors. The proposed ECM-OMP detector exhibits an error-floor for the case of $N_r = 64$ in Fig. 7 (a). This is because when too many errors are encountered by the OMP detector, our ECM assisted OMP detector fails to correct all the erroneous messages for the case of $N_r = 64$. Fortunately, by increasing N_r, the error correction capability of our ECM assisted CS detector is improved. Observe from Fig. 7 (b) that the performance of both the proposed ECM-OMP and ECM-CoSaMP detectors approach that of the MP detector and the theoretical ML limit at high SNRs [3] for the case of $N_u = 16, N_r = 128$.

Next, Fig. 8 compares the performances of different detectors for massive SM-VBLAST systems having (N_t, N_u, N_r)=(120,30,64) and (160,40,128), respectively. The performances of the VBLAST systems having $N_t = 30, N_r = 128, M = 16$ and $N_t = 40, N_r = 128, M = 16$ are added as benchmarkers. Observe from Fig. 8 (a) that both the proposed ECM-OMP and ECM-CoSaMP detectors approach the MP and ML detectors for the case of $N_u = 30$, $N_r = 128$. However, for the case of $N_u = 40$, $N_r = 128$ we observe in Fig. 8 (b) that the proposed ECM-CoSaMP detector still approaches the ML detector's performance and outperforms the conventional MP, CoSaMP, MMSE and OMP detectors. Since the N_u is very large, the proposed ECM-OMP detector exhibits an error-floor.

To provide further insights, Fig. 9 compares the performance of different detectors for the massive SM-VBLAST systems having (N_t, N_u, N_r)=(240,60,256) and (320,80, 256), respectively. The performance of the VBLAST systems having $N_t = 60, N_r = 256, M = 16$ and $N_t = 80, N_r = 256, M = 16$ are added as benchmarkers. Observe from Fig. 9 that our ECM scheme works efficiently for the case of $N_r = 256$. Specifically, the performance of the proposed ECM-CoSaMP detector is always capable of approaching that of the MP and ML detectors. More importantly, the performance of the proposed ECM-OMP

[3] According to Figs. 6-8, it becomes clear that the analytical upper bound of ABEP only becomes tight at high SNRs. This is because the value of PEP in (9) may be inaccurate at low SNRs, hence resulting in the value of $\sum_{j=2}^{2^B} P(\mathbf{x}^1 \rightarrow \mathbf{x}^j)$ being much higher than 1.

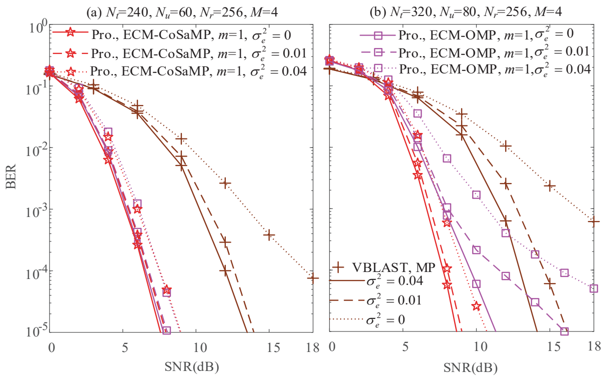

Fig. 10. Performance comparisons of the SM-VBLAST relying on the proposed detectors and of VBLAST systems relying on the MP based detectors at different channel estimation errors. The setups are the same as those of Fig. 9.

has only about 2 dB performance loss over the MP and ML detectors for the case of $N_u = 80, N_r = 256$.

Fig. 10 compares the performance of SM-VBLAST systems relying on the proposed detectors and the classic VBLAST systems relying on the MP based detector at different channel estimation errors. The setups are the same as that of Fig. 9. According to [28] of the revised manuscript, the estimated channel having errors can be modeled as

$$\tilde{\mathbf{H}} = \mathbf{H} + \mathbf{H}_e \tag{70}$$

where $\mathbf{H}_e \in \mathbb{C}^{N_r \times N_t}$ denotes the error matrices, whose elements follow the complex Gaussian distributions $\mathcal{CN}\left(0, \sigma_e^2\right)$.

Fig. 10 compares the performance of SM-VBLAST system based on the proposed detectors and the MP detector based classic VBLAST system at different channel estimation errors. The setups are identical to those of Fig. 9. Observe from Fig. 10 that SM-VBLAST systems based on the proposed ECM-CoSaMP and ECM-OMP detectors are more robust to channel estimation errors than the classic VBLAST systems relying on MP based detectors in massive MIMO setups. More specifically, the performance of the proposed ECM-CoSaMP detector is still capable of approaching that of the ML detector at the channel estimation error variance of $\sigma_e^2 = 0.01$, while it only suffers from around 2 dB performance loss over the ML detector at the channel error variance of $\sigma_e^2 = 0.04$. Additionally, the proposed ECM-CoSaMP detector provides significant performance gains over conventional VBLAST having the same channel error variance. This may be because the channel orthogonality between any two columns of a massive MIMO channel matrix is more resilient to channel estimation errors than that of a small-scale MIMO setups, which is helpful for our proposed ECM-CS detectors in terms of mitigating with channel estimation errors.

Table III presents the complexity of the proposed detectors for the aforementioned setups, which is mainly dominated by the average number of error N_{avg}^e that our ECM scheme is capable of correcting. Observe from Table III that our ECM scheme corrects at least 18 and 58 erroneous indices for the case of $N_r = 128$ and $N_r = 256$, respectively. It is also shown that both the proposed ECM-CoSaMP and ECM-OMP detectors are capable of reducing the complexity to about 3.1% $\sim$ 11.92% of that of the MP detector. Furthermore, observe in Figs. 7-8 and Table II that our ECM-CS assisted massive SM-MIMO is capable of providing 6 dB performance gains over MP aided massive VBLAST at a significantly reduced complexity.

VII. Conclusions

In this paper, both the ABEP and the capacity of the massive SM-VBLAST system have been analyzed. An efficient ECM assisted CS detector has been designed for massive SM-VBLAST systems. Our simulation results have demonstrated that the proposed ECM assisted CS detector approaches the performance of the ML detector as a benefit of identifying and correcting the erroneous indices for large N_r.

VIII. Appendix

Proof of (47): $\sum\limits_{t=1}^{N_u} \varphi_t = N - 1$ with $N = 2^{\sum_{l=1}^{N_u} B_l}$.

1) $N_u = 1$, $N_1 = 2^{B_1}$, we have $\sum\limits_{t=1}^{N_u} \varphi_t = 2^{B_1} - 1 = N_1 - 1$;
2) If $N_u = K$, $N_K = 2^{\sum_{l=1}^{K} B_l}$, we have $\sum\limits_{t=1}^{K} \varphi_t = N_K - 1$. Then, for the case of $N_u = K+1$, we have $N_{K+1} = 2^{\sum_{l=1}^{K+1} B_l}$, and the value of $\sum\limits_{t=1}^{K+1} \varphi_t$ is expressed as

$$\begin{aligned}
&\sum_{t=1}^{K+1} \varphi_t = \sum_{t=1}^{K+1} \sum_{(l_1,\ldots,l_t)\in I_{K+1}^t} \prod_{i=1}^{t} \left(2^{B_{l_i}} - 1\right) \\
&= \sum_{t=1}^{K} \sum_{(l_1,\ldots,l_t)\in I_{K+1}^t} \prod_{i=1}^{t} N_{l_i}^2 + \sum_{(l_1,\ldots,l_{K+1})\in I_{K+1}^{K+1}} \prod_{i=1}^{K+1} N_{l_i}^2 \\
&= \sum_{t=1}^{K} \left[\sum_{(l_1,\ldots,l_t)\in I_K^t} \prod_{i=1}^{t} N_{l_i}^2 + N_{l_{K+1}}^2 \sum_{(l_1,\ldots,l_{t-1})\in I_K^{t-1}} \prod_{i=1}^{t-1} N_{l_i}^2 \right] + \prod_{i=1}^{K+1} N_{l_i}^2 \\
&= \sum_{t=1}^{K} \sum_{(l_1,\ldots,l_t)\in I_K^t} \prod_{i=1}^{t} N_{l_i}^2 + N_{l_{K+1}}^2 \sum_{t=1}^{K} \sum_{(l_1,\ldots,l_{t-1})\in I_K^{t-1}} \prod_{i=1}^{t} N_{l_i}^2 \\
&+ \prod_{i=1}^{K+1} N_{l_i}^2 \\
&= \sum_{t=1}^{K} \varphi_t + N_{l_{K+1}}^2 \sum_{t=1}^{K} \varphi_{t-1} + \prod_{i=1}^{K+1} N_{l_i}^2 \\
&= \sum_{t=1}^{K} \varphi_t + N_{l_{K+1}}^2 \left[\sum_{t=1}^{K} \varphi_t + \varphi_0 - \varphi_K \right] + \prod_{i=1}^{K+1} N_{l_i}^2 \\
&= \left(N_{l_{K+1}}^2 + 1\right) \sum_{t=1}^{K} \varphi_t + N_{l_{K+1}}^2 - \prod_{i=1}^{K+1} N_{l_i}^2 + \prod_{i=1}^{K+1} N_{l_i}^2 \\
&= 2^{B_{l_{K+1}}} \left(2^{\sum_{l=1}^{K} B_l} - 1\right) + \left(2^{B_{l_{K+1}}} - 1\right) \\
&= N_{K+1} - 1
\end{aligned} \tag{71}$$

3) Based on the analysis of 1) and 2), it is concluded that (47) holds true for any number of N_u.

References

[1] L. Xiao, Y. Xiao, C. Xu, X. Lei, P. Yang, S. Li, and L. Hanzo, "Compressed-sensing assisted spatial multiplexing aided spatial modulation," *IEEE Trans. Wireless Commun.*, vol. 17, no. 2, pp. 794-807, Feb. 2018.

[2] A. Chockalingam and B. S. Rajan, Large MIMO systems. Cambridge, U.K.: Cambridge Univ. Press, 2014.

[3] F. Rusek, D. Persson, B. K. Lau, E. G. Larsson, T. L. Marzetta, O. Edfors, and F. Tufvesson, "Scaling up MIMO: Opportunities and challenges with very large arrays," *IEEE Signal Process. Mag.*, vol. 30, no. 1, pp. 40-60, Jan. 2013.

[4] P. W. Wolniansky, G. J. Foschini, G. D. Golden, and R. A. Valenzuela, "V-BLAST: An architecture for realizing very high data rates over the rich-scattering wireless channel," in Proc. *URSI Int. Symp. Signals Syst. Electron.*, Pisa, Italy, 1998, pp. 295-300.

[5] O. Shental, S. Venkatesan, A. Ashikhmin, and R. A. Valenzuela, "Massive BLAST: An architecture for realizing ultra-high data rates for large-scale MIMO,"*IEEE Wireless Commun. Lett.*, vol. 7, no. 3, pp. 404-407, Jun. 2018.

[6] S. M. Alamouti, "A simple transmitter diversity scheme for wireless communications," *IEEE J. Select. Areas Commun.*, vol. 16, no. 8, pp. 1451-1458, Oct. 1998.

[7] R. Mesleh, H. Haas, S. Sinanovic, C. W. Ahn, and S. Yun, "Spatial modulation," *IEEE Trans. Veh. Technol.*, vol. 57, no. 4, pp. 2228-2241, Jul. 2008.

[8] J. Wang, S. Jia, and J. Song, "Generalised spatial modulation with multiple active transmit antennas and low complexity detection scheme," *IEEE Trans. Wireless Commun.*, vol. 11, no. 4, pp. 1605-1615, Apr. 2012.

[9] P. Yang, M. Di Renzo, Y. Xiao, S. Q. Li, and L. Hanzo, "Design guidelines for spatial modulation," *IEEE Commun. Surveys Tuts.*, vol. 17, no. 1, pp. 6-26, First Quart. 2015.

[10] P. Yang, Y. Xiao, Y. L. Guan, K. V. S. Hari, A. Chockalingam, S. Sugiura, H. Haas, M. Renzo, C. Masouros, Z. Liu, L. Xiao, S. Li, and L. Hanzo, "Single-carrier spatial modulation: A promising design for large-scale broadband antenna systems," *IEEE Commun. Surveys Tuts.*, vol. 18, no. 3, pp. 1687-1716, Feb. 2016.

[11] L. He, J. Wang, J. Song, and L. Hanzo, "On the multi-user, multi-cell massive spatial modulation uplink: How many antennas for each user?," *IEEE Trans. Wireless Commun.*, vol. 16, no. 3, pp. 1437-1451, Dec. 2016.

[12] P. Patcharamannepakorn, S. Wu, C. Wang, E. M. Aggoune, M. M. Alwakeel, X. Ge, and M. Di. Renzo, "Spectral, energy, and economic efficiency of 5G multicell massive MIMO systems with generalized spatial modulation", *IEEE Trans. Veh. Technol.*, vol. 65, no. 12, pp. 9715-9731, Dec. 2016.

[13] L. He, J. Wang, and J. Song, "On massive spatial modulation MIMO: Spectral efficiency analysis and optimal system design," *IEEE Globecome* 2016.

[14] L. He, J. Wang, and J. Song, "Multiuser detection for FEC-Coded massive spatial modulation MIMO: An iterative interference rejection Approach," *IEEE Trans. Veh. Technol.*, vol. 66, no. 10, pp. 9567-9571, Oct. 2017.

[15] Y. Sun, J. Wang, L. He, and J. Song, "Uplink spectral efficiency analysis and optimization for massive SC-SM MIMO with frequency domain detection," *IEEE Trans. Veh. Technol.*, vol. 67, no. 5, pp. 3937-3949, May, 2018.

[16] L. He, J. Wang, J. Song, and L. Hanzo, "Bandwidth efficiency maximization for single-cell massive spatial modulation MIMO: An adaptive power allocation perspective," *IEEE Access*, vol. 5, pp. 1482-1495, Jan. 2017.

[17] T. Narasimhan, P. Raviteja, and A. Chockalingam, "Large-scale multiuser SM-MIMO versus massive MIMO," *IEEE Information Theory and Applications Workshop*, USA, pp. 1-9, 2014.

[18] S. Wang, Y. Li, and J. Wang, "Multiuser detection in massive spatial modulation MIMO with low-resolution ADCs," *IEEE Trans. Wireless Commun.*, vol, 14, no. 4, pp. 2156-2168, Apr. 2015.

[19] T. Lakshmi Narasimhan, P. Raviteja, and A. Chockalingam, "Generalized spatial modulation in large-scale multiuser MIMO systems," *IEEE Trans. Wireless Commun.*, vol. 14, no. 7, pp. 3764-3779, July, 2015.

[20] S. Wang, Y. Li, M. Zhang, and J. Wang, "Energy-efficient and low-complexity uplink transceiver for massive spatial modulation MIMO," *IEEE Trans. Veh. Technol.*, vol. 64, no. 10, pp. 4617-4632, Oct. 2015.

[21] A. G. Rodriguez and C. Masouros, "Low-complexity compressive sensing detection for spatial modulation in large-scale multiple access channels," *IEEE Trans. Commun.*, vol. 63, no. 7, pp. 2565-2579, July 2015.

[22] Z. Gao, L. Dai, Z. Wang, S. Chen, and L. Hanzo, "Compressive sensing based multiuser detector for the large-scale SM-MIMO uplink," *IEEE Trans. Veh. Technol.*, vol. 65, no. 10, pp. 8725-8730, Oct. 2016.

[23] K. Xu, H. Yu, and Y. Zhu, "Channel-adapted spatial modulation for massive MIMO visible light communications," *IEEE Photonics Technol. Lett.* vol. 28, no. 23, pp. 2693-2696, Oct. 2016.

[24] Y. Chen, L. Wang, Y. Ai, B. Jiao, and L. Hanzo, "Performance analysis of NOMA-SM in vehicle-to-vehicle massive MIMO channels," *IEEE J. Select. Areas Commun.*, vol. 35, no. 12, pp. 2653-2666, Dec. 2017.

[25] S. Wang, W. Li, and J. Lei, "Physical-layer encryption in massive MIMO systems with spatial modulation," *China Commun.*, vol. 15, no. 10, pp. 159-171, Oct. 2018.

[26] H. Noh, Y. Kim, J. Lee, and C. Lee, "Codebook design of generalized space shift keying for FDD massive MIMO systems in spatially correlated channels," *IEEE Trans. Veh. Technol.*, vol. 64, no. 2, pp. 513-523, Feb. 2015.

[27] Y. Cui and X. Fang, "Performance analysis of massive spatial modulation MIMO in high-speed railway," *IEEE Trans. Veh. Technol.*, vol. 65, no. 11, pp. 8925-8932, Nov. 2016.

[28] L. Xiao, Y. Xiao, Y. Zhao, P. Yang, M. D. Renzo, S. Q. Li and W. Xiang, Time domain turbo equalization for single-carrier aided generalized spatial modulation systems, *IEEE Trans. Wireless Commun.*, vol. 16, no. 9, pp. 5702-5716, 2017.

[29] Z. Gao, L. Dai, C. Qi, C. Yuen, and Z. Wang, "Near-optimal signal detetcor based on structured compressive sensing for massive SM-MIMO," *IEEE Trans. Veh. Technol.*, vol. 66, no. 2, pp. 1860-1865, Feb. 2017.

[30] N. Ishikawa and S. Sugiura, "Rectangular differential spatial modulation for open-loop noncoherent massive-MIMO downlink," *IEEE Trans. Wireless Commun.*, vol. 16, no. 3, pp. 1908-1920, Mar. 2017.

[31] M. Arisaka and S. Sugiura, "Energy-versus-bandwidth-efficiency tradeoff in spatially modulated massive MIMO downlink," *IEEE Wireless Commun. Lett.*, vol. 8, no. 1, pp.197-200, Feb. 2019.

[32] N. Ishikawa, R. Rajashekar, C. Xu, S. Sugiura, and L. Hanzo, "Differential space-time coding dispensing with channel estimation approaches the performance of its coherent counterpart in the open-loop massive MIMO-OFDM downlink," *IEEE Trans. Commun.*, vol. 66, no. 2, pp. 6190-6204, Dec. 2018.

[33] M. Maleki, H. R. Bahrami, and A. Alizadeh, "Layered spatial modulation for multiuser communications," *IEEE Trans. Wireless Commun.*, vol. 15, no. 10, pp. 7143-7159, Oct. 2016.

[34] M. Maleki, K. M, Pour, and M. Soltanalian, "Receive spatial modulation in correlated massive MIMO with partial CSI," *IEEE Trans. on Signal Process.*, vol. 67, no. 5, pp. 1237-1250, March, 2019.

[35] T. L. Narasimhan and A. Chockalingam, "On the capacity and performance of generalized spatial modulation," *IEEE Commun. Lett.*, vol. 20, no. 2, pp. 252-255, Nov. 2015.

[36] W. Qu, M. Zhang, X. Cheng, and P. Ju, "Generalized spatial modulation with transmit antenna grouping for massive MIMO," *IEEE Access*, vol. 5, pp. 26798-26807. Nov. 2017.

[37] Z. An, J. Wang, J. Wang, and J. Song, "Mutual information and error probability analysis on generalized spatial modulation system", *IEEE Trans. Commun.* vol. 65, no. 3, pp. 1044-1060, Mar. 2017.

[38] A. I. Ibrahim, T. Kim, and D. J. Love, "On the achievable rate of generalized spatial modulation using multiplexing under a Gaussian mixture model," *IEEE Trans. commun.*, vol. 64, no. 4, pp. 1588-1599, Jan. 2016.

[39] Z. Gao, L. Dai, S. Han, C. L, Z. Wang, and L. Hanzo, "Compressive sensing techniques for next-generation wireless communications," *IEEE Wireless Commun.*, vol. 25, no. 3, pp. 144-153, June, 2018.

[40] L. Xiao, P. Yang, Y. Xiao, S. Fan, M. Di. Renzo, W. Xiang, and S. Li, "Efficient compressive sensing detectors for generalized spatial modulation systems," *IEEE Trans. Veh. Technol.*, vol. 66, no. 2, pp. 1284-1298, Feb. 2017.

[41] S. S. Chen, D. L. Donoho, and M. A. Saunders, "Atomoic decomposition by basis pursuit," *SIAM Review*, vol. 43, no. 1, pp. 129-159, Feb. 2001.

[42] J. Tropp and A. Gilbert, "Signal revorery from random measurements via orthogonal matching pursuit," *IEEE Trans. Inf. Theroy*, vol. 53, no. 12, pp. 4655-4666, Dec. 2007.

[43] D. Needell and J. A. Tropp, "CoSaMP: Iterative signal recover from incomplete and inaccurate samples," *Applied and Computaional Harmonic Analysis*, vol. 26, no. 3, pp. 301-321, May, 2009.

[44] S. Kwon, J. Wang, and B. Shim, "Multipath matching pursuit," *IEEE Trans. Inf. Theroy*, vol. 60, no. 5, pp. 2986-3001, May, 2014.

[45] D. Wipf and B. D. Rao, "An empirical bayesian strategy for solving the simultaneous sparse approximation problem," *IEEE Trans. Signal Process.*, vol. 55, no. 7, pp. 3704-3716, July, 2007.

[46] D. L. Donoho, A. Maleki, and A. Montanari, "Message passing algorithms for compressed sensing," Proc. Nat. Acad. Sci., vol. 106, pp. 18914-18919, 2009.

[47] O. Oyman, R. Nabar, H. Bolcskei, and A. J. Paulraj, "Characterizing the statistical properties of mutual information in MIMO channels," *IEEE Trans. Signal. Process.*, vol. 51, no. 11, pp. 2784-2795, Nov. 2003.

Lixia Xiao received the B.E., M.E., and Ph. D degrees in 2010, 2013 and 2017, respectively from University of Electronic Science and Technology of China (UESTC). Currently, she is a research fellow with the department of Electrical Electronic Engineering of University of Surrey. Her research is in the field of wireless communications and communication theory. In particular, she is very interested in signal detection and performance analysis of wireless communication systems.

Pei Xiao (SM'11) is a professor of Wireless Communications at the Institute for Communication Systems, home of 5G Innovation Centre (5GIC) at the University of Surrey. He is the technical manager of 5GIC, leading the research team at on the new physical layer work area, and coordinating/supervising research activities across all the work areas within 5GIC (www.surrey.ac.uk/5gic research). Prior to this, he worked at Newcastle University and Queen's University Belfast. He also held positions at Nokia Networks in Finland. He has published extensively in the fields of communication theory and signal processing for wireless communications.

Zilong Liu is a Lecturer at the School of Computer Science and Electronic Engineering, University of Essex, UK. From January 2018 to November 2019, he was a Senior Research Fellow at the Institute for Communication Systems (ICS), Home of the 5G Innovation Centre (5GIC), University of Surrey, UK. Prior moving to UK, he spent 9.5 years in the School of Electrical and Electronic Engineering, Nanyang Technological University (NTU), Singapore, first as a Research Associate (since July 2008) and then a Research Fellow (since November 2014). He received his PhD in June 2014 with a thesis entitled "Perfect- and Quasi- Complementary Sequences" advised by Prof. Guan Yong Liang. He is generally interested in coding and signal processing for various communication systems, with emphasis on signal design and algebraic coding, error correction codes, iterative receiver design, robust/efficient multiple access communications, and physical layer implementation/prototyping of communications systems. Details of his research can be found at: https://sites.google.com/site/zilongliu2357

Wenjuan Yu received the Ph.D. degree in communication systems from the School of Computing and Communications, Lancaster University, Lancaster, UK, in 2018. She is currently a Research Fellow with 5G Innovation Centre, Institute for Communication Systems, University of Surrey, Guildford, UK. Her research interests include radio resource management, uRLLC, 5G and beyond (B5G) wireless networks. She is an Executive Editor of the Transactions on Emerging Telecommunications Technologies.

Harald Haas received the PhD degree from the University of Edinburgh in 2001. He currently holds the Chair of Mobile Communications at the University of Edinburgh, and is the founder and Chief Scientific Officer of pureLiFi Ltd as well as the Director of the LiFi Research and Development Center at the University of Edinburgh. His main research interests are in LiFi and visible light communications. He first introduced and coined 'spatial modulation' and 'LiFi'. The latter was listed among the 50 best inventions in TIME Magazine 2011. Prof. Haas was an invited speaker at TED Global 2011, and his talk: "Wireless Data from Every Light Bulb" has been watched online more than 2.5 million times. He gave a second TED Global lecture in 2015 on the use of solar cells as LiFi data detectors and energy harvesters. This has been viewed online more than 2 million times. He has published more than 400 conference and journal papers including a paper in Science. Prof. Haas is editor of IEEE Transactions on Communications and IEEE Journal of Lightwave Technologies. He was co-recipient of recent best paper awards at VTC-Fall, 2013, VTC-Spring 2015, ICC 2016 and ICC 2017. He was co-recipient of the EURASIP Best Paper Award for the Journal on Wireless Communications and Networking in 2015, and co-recipient of the Jack Neubauer Memorial Award of the IEEE Vehicular Technology Society. In 2012 and 2017, he was the recipient of the prestigious Established Career Fellowship from the EPSRC (Engineering and Physical Sciences Research Council) within Information and Communications Technology in the UK. In 2014, he was selected by EPSRC as one of ten RISE (Recognising Inspirational Scientists and Engineers) Leaders in the UK. In 2016, he received the outstanding achievement award from the International Solid State Lighting Alliance. He was elected a Fellow of the Royal Society of Edinburgh in 2017, and was elevated to Fellow of the IEEE in 2017.

Lajos Hanzo (http://www-mobile.ecs.soton.ac.uk) FREng, F'04, FIET, Fellow of EURASIP, received his 5-year degree in electronics in 1976 and his doctorate in 1983 from the Technical University of Budapest. In 2009 he was awarded an honorary doctorate by the Technical University of Budapest and in 2015 by the University of Edinburgh. In 2016 he was admitted to the Hungarian Academy of Science. During his 40-year career in telecommunications he has held various research and academic posts in Hungary, Germany and the UK. Since 1986 he has been with the School of Electronics and Computer Science, University of Southampton, UK, where he holds the chair in telecommunications. He has successfully supervised 119 PhD students, co-authored 18 John Wiley/IEEE Press books on mobile radio communications totalling in excess of 10 000 pages, published 1800+ research contributions at IEEE Xplore, acted both as TPC and General Chair of IEEE conferences, presented keynote lectures and has been awarded a number of distinctions. Currently he is directing a 60-strong academic research team, working on a range of research projects in the field of wireless multimedia communications sponsored by industry, the Engineering and Physical Sciences Research Council (EPSRC) UK, the European Research Council's Advanced Fellow Grant and the Royal Society's Wolfson Research Merit Award. He is an enthusiastic supporter of industrial and academic liaison and he offers a range of industrial courses. He is also a Governor of the IEEE ComSoc and VTS. He is a former Editor-in-Chief of the IEEE Press and a former Chaired Professor also at Tsinghua University, Beijing. For further information on research in progress and associated publications please refer to http://www-mobile.ecs.soton.ac.uk